The role of blood-borne factors in triggering atypical astrocytes

Kijana Kaaria George

Dissertation submitted to the faculty of Virginia Polytechnic Institute and State University in partial fulfillment of the requirements for a degree of

Doctor of Philosophy

In

Translational Biology, Medicine, and Health

Stefanie Robel, Chair

Michelle Olsen

Matthew Buczynski

Robert Gourdie

14 March 2022

Roanoke, Virginia

Keywords: astrocyte, blood-brain barrier, leakage, astrogliosis, traumatic brain injury

The role of blood-borne factors in triggering atypical astrocytes

Kijana Kaaria George

ABSTRACT

Mild traumatic brain injury (mTBI)/ concussion accounts for 70-90% of all reported TBI cases in the United States and can cause long-term neurological outcomes that negatively impact quality of life. Previous studies revealed that increased blood-brain barrier (BBB) leakage is correlated with poor neurological outcomes after mTBI, yet the biological mechanisms linking BBB damage to the onset of neurological deficits after mTBI are not well understood. Previously, we found that astrocytes lose expression of homeostatic proteins after mTBI, characterizing the changes in astrocytic protein expression as an "atypical astrocyte response." Yet, the upstream mechanisms that induce this atypical astrocyte response after mTBI have yet to be elucidated. In models of more severe TBI, exposure to blood-borne factors triggers astrogliosis via upregulation in markers, such as glial fibrillary acidic protein (GFAP), but how exposure to blood-borne factors affects astrocyte protein expression in the context of mTBI is not well understood. Therefore, we hypothesized that mTBI-induced BBB damage causes atypical astrocytes via exposure to blood-borne factors. To test this hypothesis, we use a mTBI mouse model, two-photon microscopy, an endothelial cell-specific genetic ablation model, and serum-free primary astrocyte cultures. Here, we found that mTBI causes BBB damage through the loss of proteins involved in maintaining the BBB's physical and metabolic barriers, and BBB damage is sustained long-term after injury. Also, we demonstrated that leakage of blood-borne factors is sufficient to trigger atypical astrocytes, and plasma exposure triggers a similar response *in vitro*. Overall, these findings suggest that mTBI induces long-term BBB damage, and exposure to blood-borne factors triggers the loss of key homeostatic astrocytic proteins involved in maintaining healthy neuronal function.

The role of blood-borne factors in triggering atypical astrocytes

Kijana Kaaria George

GENERAL AUDIENCE ABSTRACT

Mild traumatic brain injury (mTBI)/ concussion makes up 70-90% of all TBI cases reported in the United States and is commonly observed after car crashes, sports-related tackles, and blast exposure during military combat. People who experience mTBI develop debilitating long-term neurological consequences, such as sleep disturbances, depression, and dementia. Clinical data suggests mTBI causes damage to the barrier between the brain and blood, known as the blood-brain barrier (BBB). This damage has been correlated to the onset of poor neurological deficits, yet how damage to this barrier is causally linked to long-term neurological consequences remains to be fully understood. In our lab, we found that mTBI causes loss of proteins important for maintaining a healthy environment in the brain in specialized cells called astrocytes. However, the biological events that trigger the loss of protein expression in astrocytes after mTBI have yet to be fully investigated. Thus, we hypothesized that mTBI causes loss of these proteins via leakage of blood-borne factors. To test this hypothesis, we used a mTBI mouse model, two-photon microscopy, genetic manipulation, and cell cultures. In our studies, we found that mTBI triggers BBB damage via loss of proteins that make up its protective properties. Also, we demonstrated that leakage of blood-borne factors is sufficient to cause loss of astrocyte-specific proteins both in brain and cell cultures. Altogether, we show that a single mTBI is sufficient to cause loss of astrocyte-specific protein expression via exposure to blood-borne factors. These findings may point to targeting either the blood-borne factor(s) or their corresponding receptor pathways in astrocytes to halt the progression of long-term neurological deficits after mTBI.

Acknowledgements

I would like to thank Dr. Stefanie Robel for giving me the opportunity to work in her lab for the last several years. I am grateful for her investment in both my professional and personal development as a graduate student. Through all the accomplishments and challenges I have experienced throughout my time at Virginia Tech, she has been supportive of my way of navigating through these successes and failures. I appreciate her knowledge in all topics related to glial biology and how they play a role in brain pathology, as well as her commitment to allowing me to mature both as a scientist and as a human being.

I would also like to thank Dr. Michelle Olsen, Dr. Matthew Buczynski, and Dr. Robert Gourdie: their different areas of expertise helped me think about my project from different perspectives.

I am grateful for Dr. Ben Heithoff, Dr. Carmen Muñoz-Ballester, Dr. Alex Shandra, Ivan Zuidhoek, Dzenis Mahmutovic, and all the undergraduate and post-baccalaureate students for making the lab an engaging and exciting place to work. Through our ups and downs, we have stayed committed to fostering teamwork and creativity in solving the major gaps in knowledge in glial biology.

To all the TBMH coordinators, colleagues within my TBMH cohort, vivarium staff, principal investigators, and any member of FBRI that I had the pleasure of knowing, I thank all of you for letting me know in everyone's individual ways that graduate school is more than just conducting experiments and writing papers.

Lastly, this entire journey would not have been possible without my family. I want to thank God, my mom, my dad, my sister Ameeka, and my grandparents for always being abundant sources of unconditional love and support. Through all the challenges I have experienced growing up and the sacrifices they have made, they continue to grant me the strength to face anything life puts in my path and to overcome these obstacles with humility, grace, and steadiness.

Table of Contents

Acknowledgements iv

List of Figures and Tables ix

Abbreviations xi

1 Introduction/Review of Literature 1

1.1 The majority of cases of traumatic brain injury (TBI) are classified as mild concussive TBI 1

1.2 Blood-brain barrier (BBB) leakage has been linked to long-term neurological consequences after mild concussive TBI 2

1.3 What does exposure to blood do to the brain? 3

1.4 Differences between focal TBI and mild TBI/ concussion 4

1.5 Astrocytes are active cellular players that promote healthy central nervous system (CNS) function 5

1.5.1 How do astrocytes respond to focal TBI? 6

1.5.1.1 Consequences of astrocyte reactivity 6

1.5.1.2 Blood-borne factors that trigger astrogliosis after TBI 6

1.5.2 How do astrocytes respond to mild TBI/ concussion 7

2 Materials and Methods 9

2.1 Mice 9

2.1.1 Mouse strains 9

2.1.2 Weight-drop 9

2.1.3 Two-photon microscopy 10

2.1.4 Experimental design for endothelial cell (EC) ablation 11

2.1.5 Tamoxifen administration 11

2.1.6 Cadaverine/dextran administration 11

2.2 Histology 12
2.3 Primary astrocyte cell culture 12
2.3.1 Cardiac puncture 14
2.3.2 Heat-denaturation 14
2.3.3 Treatment of blood-borne factors in vitro 15
2.4 Immunocytochemistry 15
2.5 Data analysis 15
2.5.1 Quantification of Glt1 Loss 15
2.5.2 Quantification of Cadaverine Leakage 15
2.5.3 Quantification of ZO-1 16
2.5.4 Quantification of GLUT1 16
2.5.5 Quantification of Glt1/Kir4.1 in vitro 16
2.5.6 Quantification of CD45+ cells in the cortex 17
2.5.7 Quantification of area coverage of CD31+ blood vessels 17
2.5.8 Quantification of β-dystroglycan 17
2.5.9 Quantification of AQP4 18
2.5.10 Quantification of MMP9 18
2.5.11 Quantification of pSMAD2 18
2.6 Statistics 18
2.6.1 For All Data Sets 18
2.6.2 Poisson Distribution for CD45+ data 19
3 Results 20
3.1 Loss of astrocytic proteins correlates with long-term neurological consequences after mTBI 20

3.2 Significant BBB leakage, with minimal vessel rupture, occurs as early as 1 day after mTBI 22

3.3 mTBI triggers the loss of proteins responsible for maintaining BBB properties 26

3.4 Leakage of blood-borne factors is sufficient to trigger atypical astrocytes 28

3.4.1 EC ablation reduces the expression of proteins involved in maintaining BBB properties and induces an atypical astrocytes response 28

3.5 Development of a serum-free culture system to test the effect of blood-borne factors 34

3.5.1 Plasma treatment triggers the atypical astrocyte phenotype in vitro at 24 hours 34

3.5.2 Treatment of primary astrocytes with plasma maintained on 12 mm and 8 mm coverslips 36

3.5.3 Significant loss in Glt1/Kir4.1 expression in primary astrocytes maintained in media for 14 days at 24 hours 38

3.6 Exposure to plasma in primary astrocyte cell culture mimics the atypical astrocyte response in vitro 40

3.7 BBB leakage is not repaired after mTBI 48

3.7.1 BBB leakage is sustained at 64 days after mTBI 48

3.7.2 BBB properties remain disrupted at 64 days after mTBI 48

3.8 Loss of astrocytic factors that maintain BBB integrity occurs after mTBI 51

4 Discussion 58

4.1 mTBI is sufficient to trigger BBB damage 58

4.2 Does the primary astrocyte culture model mimic what is observed after mTBI? 58

4.3 What plasma-borne factors trigger atypical astrocytes? 60

4.4 What downstream signaling pathways are activated after blood-borne factor leakage? 62

4.5 How do astrocytes maintain BBB integrity after mTBI? 64

4.6 The BBB fails to repair itself after mTBI 66

5 References 67

List of Figures and Tables

Figure 1. Increased area containing atypical astrocytes is correlated with likelihood of developing PTE after mTBI 20

Figure 2. BBB leakage overlaps with the loss of astrocytic markers Glt-1, Kir4.1, S100β and Aldh1l1-eGFP 21

Figure 3. Blood-brain barrier leakage occurs in areas of atypical astrocytes after mTBI 23

Figure 4. mTBI does not cause significant vessel rupture.....25

Figure 5. The blood-brain barrier is damaged after mTBI.....27

Figure 6. EC ablation in the BBB is sparse after Tx administration 30

Figure 7. BBB leakage induced via EC specific genetic ablation is sufficient to trigger atypical astrocytes in the absence of mTBI. 32

Figure 8. Exposure to plasma triggered reduced Glt1/Kir4.1 expression after 24 hours in primary astrocytes maintained in serum-free media for 7 d*iv* 35

Figure 9. Exposure to fresh mouse plasma causes reduction in Glt1/Kir4.1 in primary astrocyte cultures maintained in serum-free media for 7 d*iv*, regardless of coverslip size 37

Figure 10. Astrocytes maintained in media for different lengths of time experience loss of Glt1/Kir4.1 signal intensity after plasma exposure 39

Figure 11. Glt1 and Kir4.1 expression in astrocytes is reduced 24 hours after plasma treatment *in vitro* and is triggered by a plasma protein(s).....42

Figure 12. Fibrinogen triggers Glt1, but not Kir4.1 loss *in vitro* 43

Figure 13. Albumin triggers Glt1, but not Kir4.1 loss *in vitro*..... 45

Figure 14. mTBI causes increased TGF- β signaling in atypical astrocytes.....47

Figure 15. The BBB is not repaired after mTBI 49

Figure 16. BBB leakage induces loss of astrocytic-secreted proteins responsible for BBB maintenance after mTBI.....53

Figure 17. Basement membrane proteins are lost after mTBI 55

Figure 18. mTBI does not cause changes in MMP9 expression. 56

Figure 19. Diagram of the TGF- β signaling pathway.....64

Table 1. List of blood-borne factors and their molecular weights.....4

Table 2. List of astrocytic proteins and the changes in protein expression observed in immunohistochemistry in response to mTBI.....8

Table 3. Summary of changes in astrocytic protein expression observed in ICC after treatment.....61

Abbreviations

ACSA-2: astrocyte cell-specific antibody-2

AQP4: aquaporin-4

BBB: blood-brain barrier

bDG: β -dystroglycan

BSA: bovine serum albumin

CNS: central nervous system

CT: Computed Topography

Cx43: connexin 43

DAGC: dystrophin-associated glycoprotein complex

DAPI: 4,6-diamidino-2-phenylindole

dpa: day(s) post administration

dpi: day(s) post injury

DTA: diptheria toxin A

EC: endothelial cell

ECM: extracellular matrix

FBS: fetal bovine serum

GFAP: glial fibrillary acidic protein

Glt1: glutamate transporter-1

GLUT1: glucose transporter-1

hpa: hour(s) post-administration

ICAM-1: intercellular adhesion molecule 1

ICC: immunocytochemistry

IgG: immunoglobulin G

IHC: immunohistochemistry

IL-6: interleukin-6

MACS: magnetic-activated cell sorting

MMP9: matrix metalloproteinase-9

mpi: minute(s)post injury

MRI: magnetic resonance imaging

MS: multiple sclerosis

mTBI: mild traumatic brain injury

PAR: protease-activated receptor

PBS: phosphate buffer saline

PFA: parafolmadehyde

PTE: post-traumatic epilepsy

ROCK: rho kinase

ROI: region of interest

ROS: reactive oxidative species

Shh: sonic hedgehog

SMURF: SMAD ubiquitin regulatory factor

TGF- β: transforming-growth factor beta

TNF- α: tumor necrosis factor alpha

TrkB: tyrosine receptor kinase B

Tx: tamoxifen

ZO-1: zonula occludens

1 Introduction/Review of Literature

1.1 The majority of cases of traumatic brain injury (TBI) are classified as mild concussive TBI

Every year, about 1.7-3.8 million people sustain traumatic brain injuries (TBIs) in the United States. As a result, about 280,000 people are hospitalized each year due to injuries sustained from the impact (Leitner et al., 2021). Immediately after TBI, people can experience symptoms that tend to resolve in the span of a few days, including loss of consciousness and altered motor function. In other cases, people who experience TBI can develop long-term neurological consequences associated with TBI, such as memory loss, lack of concentration, and sleep and behavioral disturbances (Bolton-Hall, Hubbard, & Saatman, 2019; Ellis, Leddy, Cordingley, & Willer, 2018; Kenzie et al., 2018), which can negatively impact the quality of life for those affected.

Out of all TBI cases reported, about 70-90% are classified as mild TBI (mTBI)/ concussions which are commonly observed after car crashes, blast exposure, and sports-related injury (Cassidy et al., 2004). While most people who experience mTBI are not admitted to the hospital immediately after impact, about 10-40% of people develop long-term neurological consequences (Fehily & Fitzgerald, 2017). Typically, mTBI does not result in detectable signs of focal lesions in the brain that can be identified via standard imaging techniques, including magnetic resonance imaging (MRI) and computed tomography (CT) scans (Pavlovic, Pekic, Stojanovic, & Popovic, 2019). However, these patients who sustain mTBI can develop long-term neurological consequences, similar to what is observed after more severe TBIs, suggesting that underlying biological mechanisms may trigger the development of secondary brain injury, such as cerebral edema and hyperexcitability in response to mTBI (Johnson et al., 2013). However, the different biological mechanisms and how they induce the development of secondary brain injury after mTBI are not well understood.

1.2 Blood-brain barrier (BBB) leakage has been linked to long-term neurological consequences after mild concussive TBI

The blood-brain barrier (BBB) is a protective interphase that separates the brain parenchyma from the periphery. One of the major hallmarks of the BBB – a hallmark that makes the endothelial cells (ECs) that form cerebral blood vessels different from peripheral blood vessels – is the presence of tight junctions, which are responsible for preventing foreign blood-borne factors and pathogens from entering the brain parenchyma. Another key characteristic of the BBB is that it is also a metabolic barrier, which contains transporters that allow for the selective exchange of nutrients, ions, and proteins between the brain and the periphery. Lastly, the BBB contains low expression leukocyte adhesion molecules, which reduce transcytosis of peripheral immune cells into the brain parenchyma (Obermeier, Daneman, & Ransohoff, 2013).

In addition to the BBB's physical and metabolic properties, maintenance of the BBB is regulated by the extracellular matrix (ECM), which is composed of basement membrane proteins that are responsible for structural support, cell anchoring, and signaling transduction in the ECs (Xu, Nirwane, & Yao, 2019). Also, neurons and glial cells, including astrocytes, microglia, and oligodendrocytes, interact with the ECs of the BBB and help to control BBB integrity and regulate blood flow throughout the brain (Yu, Ji, & Shao, 2020). Together, each of these components form the neurovascular unit (NVU).

For decades, clinical studies have identified BBB dysfunction as one of the early biological events that precede the onset of worsening neurological outcomes after TBI or neurodegenerative disease (Sivandzade, Alqahtani, & Cucullo, 2020; Szarka et al., 2019). With the use of dynamic contrast-enhanced MRI, researchers observed increased BBB leakage that occurs after a single mTBI (Li et al., 2014), and this leakage is sustained for several months/years, suggesting that BBB damage is linked to the development of secondary brain

injury. Yet, the causal mechanisms tying BBB damage to long-term neurological consequences after mTBI are not well understood.

1.3 What does exposure to blood do to the brain?

The development of long-term neurological consequences following BBB damage implies that the leakage of blood-borne factors contributes to the initiation of secondary brain damage in the context of TBI or disease. In the bloodstream, 55% of the total volume of blood is composed of plasma, which contains mostly water and different plasma proteins. These plasma proteins include fibrinogen, thrombin, albumin, and immunoglobulins. In response to vessel damage, fibrinogen and thrombin interact with each other to form fibrin, which repairs sites of vessel rupture. Both fibrinogen and thrombin extravasation have been linked to Alzheimer's disease and multiple sclerosis (MS) (Davalos et al., 2012; Lin et al., 2013; Sulimai & Lominadze, 2020).

Albumin makes up 65% of all plasma proteins in the blood and is responsible for transporting nutrients, ions, and other proteins throughout the bloodstream (Moman, Gupta, & Varacallo, 2021). In the context of brain pathology, albumin extravasation into the brain has been linked to epileptogenesis (Ralay Ranaivo, Hodge, Choi, & Wainwright, 2012; Ralay Ranaivo & Wainwright, 2010). Next, immunoglobulins (antibodies) are produced by B cells, which initiate cytokine production to trigger an immune response (Ransohoff, Schafer, Vincent, Blachère, & Bar-Or, 2015). Increased cytokine release, mediated by the production of immunoglobulins by B cells can cause peripheral immune cells to migrate to the brain parenchyma, initiating a neuroinflammatory response (Bush et al., 1999; Nettis & Pariante, 2020). For example, increased immunoglobulin G (IgG) circulation and the migration of B cells to the meninges are implicated in the development of MS. Whether antibodies produced from B cells trigger the onset of symptoms associated with neurodegenerative disease has yet to be fully investigated (Brimberg et al., 2015).

Iron is found in the hemoglobin of erythrocytes and is important for transporting oxygen

throughout the bloodstream. While iron provides important health benefits, such as facilitating oxygen transport and aiding in cellular respiration, elevated levels of iron can cause impaired mitochondrial respiration by causing increased production of reactive oxygen species (ROS), leading to cell death (D'Mello & Kindy, 2020). To determine how increased iron levels affect brain function, previous studies used a mouse model of intracranial hemorrhage (ICH) and treatment with inhibitors against iron, and they found that elevated iron levels trigger neurodegeneration through impaired mitochondrial function (Wan, Ren, & Wang, 2019; Wiethoff & Houlden, 2017).

Under healthy conditions, the BBB utilizes its physical and metabolic barriers to maintain normal concentrations of different ions and ensure healthy neuronal function. For example, establishing a physiological potassium ion gradient is responsible for maintaining all excitable cells' resting membrane potentials and for triggering repolarization during the generation of action potentials in neurons. In addition to its role in generating excitable conditions in the central nervous system (CNS), potassium ions are important for regulating cerebral blood flow (Nguyen, Winn, & Janigro, 2000). In response to BBB disruption, the concentration of extracellular potassium ions increases and can create hyperexcitability in neurons and reduced cerebral blood flow (Janigro, 2012).

Blood-Borne Factors	Molecular Weight (kDa)
Albumin	67 kDa
Fibrinogen	340 kDa
Thrombin	36 kDa
Immunoglobulins	150 kDa

Table 1. *List of blood-borne factors and their molecular weights*

1.4 Differences between focal TBI and mild TBI/ concussion

Focal TBI is characterized by direct brain damage that can lead to necrosis, scarring, and hemorrhaging in the brain. As a result, it can lead to debilitating neurological outcomes such as

epilepsy, paralysis, and cognitive impairment (Sharma, Tiarks, Haight, & Bassuk, 2021). Most studies examining the biological mechanisms linking TBI to such neurological consequences were performed by using focal TBI models in rodents. For example, our understanding of how blood-borne factors lead to pathological changes in the brain developed from studies where each factor was injected directly into the brain (Brown et al., 2021; Frigerio et al., 2012). While these studies help to show that leakage of different blood-borne factors contributes to brain pathology, focal TBI makes up about less than 10% of all TBI cases (Shandra et al., 2019).

mTBI is characterized by rapid acceleration-deceleration forces that account for 70-90% of all TBI cases. mTBI is commonly observed after sports-related injuries and car crashes, and typically people experience symptoms, such as loss-of-consciousness and headaches after mTBI (Fehily & Fitzgerald, 2017; Pavlovic et al., 2019). Usually, these symptoms last for a few days after impact. However, a subset of people who experience mTBI develop worsening neurological outcomes, such as chronic traumatic encephalopathy (CTE), which is characterized by progressive neurodegeneration associated with repeated concussions (Tagge et al., 2018). Since previous studies hint at BBB leakage as a contributing factor to the development of secondary injury, it is important to determine the causal mechanisms linking the leakage of different blood-borne factors and the onset of worsening neurological consequences after mTBI.

1.5 Astrocytes are active cellular players that promote healthy central nervous system (CNS) function

Astrocytes are glial cells in the CNS that interact with neuronal synapses via their astrocytic processes, which contain various transporters that remove excess neurotransmitters and ions from the extracellular space. To maintain normal excitability in neurons, astrocytes remove excess glutamate from neuronal synapses through astrocyte-specific transporters, including glutamate transporter-1 (Glt1) and GLAST. Also, astrocytes play an important role in the buffering of extracellular potassium ions through their Kir4.1 channels. In addition to communicating with neuronal synapses, they facilitate cell-to-cell communication within

astroglial networks via gap junctions (Pannasch & Rouach, 2013).

Astrocytes play a key role in maintaining BBB integrity by contacting ECs via astrocytic endfeet. The endfeet contain transporters that allow for the passage of nutrients, ions, and water between the brain parenchyma and the periphery. Also, astrocytic endfeet have been shown to regulate cerebral blood flow and secrete factors that ensure healthy tight junction function (Kubotera et al., 2019). Initially, its role in BBB maintenance was first discovered in co-cultures where ECs cultured with astrocytes displayed increased expression of proteins involved in the formation of tight junctions compared to ECs cultured on their own (Lee et al., 2003). However, we previously demonstrated that astrocytes play a crucial role in BBB integrity *in vivo* by genetically ablating a subset of astrocytes, which caused disrupted tight junction vessel coverage and increased BBB permeability (Heithoff et al., 2021).

1.5.1 How do astrocytes respond to focal TBI?

1.5.1.1 Consequences of astrocyte reactivity

In response to brain injury, astrocytes undergo changes in their morphology and function through a process called astrogliosis. The neuroprotective role of astrogliosis in response to focal TBI is well-documented: glial boundaries are formed around the primary injury site to mitigate further brain damage and neuroinflammation (Sofroniew, 2009). However, changes in the astrocytes' morphology and function in response to brain pathology can contribute to secondary injury. For example, the deletion of β-integrin to trigger astrogliosis causes the development of seizures by reducing both glutamate and potassium uptake in astrocytes (Robel et al., 2015). These findings suggest that astrogliosis can have detrimental effects on brain homeostasis in that it can compromise the astrocytes' ability to remove excess neurotransmitters and ions – a key function that is paramount for ensuring healthy neuronal activity.

1.5.1.2 Blood-borne factors that trigger astrogliosis after TBI

BBB disruption has been observed in patients with epilepsy, suggesting that the leakage

of blood-borne factors may trigger astrogliosis after the onset of disease or injury (Heinemann, Kaufer, & Friedman, 2012). Therefore, it is important to understand how astrogliosis may trigger long-term neurological consequences in the context of TBI and identify the upstream mechanisms that cause astrogliosis after injury. Some examples of the different blood-borne factors involved in initiating astrogliosis after TBI include fibrinogen, albumin, and fibrin. Fibrinogen has been shown to trigger GFAP upregulation and the production of proteoglycans that form the glial boundaries in response to focal TBI (Schachtrup et al., 2010). Denaturing fibrinogen with ancrod *in vivo* reduced the formation of glial boundaries after focal TBI. Also, fibrin causes upregulation of GFAP, tyrosine receptor kinase B (TrkB), and intercellular adhesion molecule 1 (ICAM-1) in cultured astrocytes (V. D. Clark, Layson, Charkviani, Muradashvili, & Lominadze, 2018). While thrombin has been shown to induce GFAP upregulation, it triggers the production of matrix metalloproteinase-9 (MMP9), which is involved in the degradation of basement membranes of neighboring cells and is implicated in inflammatory responses in primary astrocyte cultures (Lin et al., 2013; Mhatre et al., 2004).

In addition to iron causing neurodegeneration via increased production of ROS, it interacts with astrocytes and causes them to release pro-inflammatory cytokines, including tumor necrosis factor-alpha (TNF- α) and interleukin-6 (IL-6) (Bylicky, Mueller, & Day, 2018), and to upregulate ferritin to prevent ROS buildup. Altogether, astrocytes' responses to different blood-borne factors have been well-characterized in more severe TBI models and *in vitro* studies. However, how they respond to blood-borne factors in the context of mTBI is remains to be fully investigated.

1.5.2 How do astrocytes respond to mild TBI/ concussion

Unlike the findings observed after focal TBI, there are some areas in the cortex where astrocytes became mildly reactive but do not form glial boundaries in the cortex of mice that were subjected to mTBI (Shandra et al., 2019). To further assess how astrocytes respond to mTBI, we stain for astrocytic markers that are involved in maintaining homeostatic functions of

the brain. We observe a subset of astrocytes that had lost proteins, such as glutamate transporter-1 (Glt1), Kir4.1, S100β, connexin 43 (Cx43), and glutamine synthetase that occur as early as several minutes after mTBI. We characterize the loss of homeostatic proteins in astrocytes as an "atypical astrocyte response," and this response is sustained for months after injury, which can pose a challenge for healthy neuronal function. Before the atypical astrocyte response can be targeted to halt the progression of neurological consequences after mTBI, the upstream mechanisms inducing this response remain to be fully understood.

Astrocyte Marker	**Timepoints**							
	acute	**4hpi**	**1dpi**	**3dpi**	**7dpi**	**14dpi**	**28dpi**	**56dpi**
Kir 4.1	NA	↓	NA	NA	↓	↓	NA	NA
Glt1	↓	↓	↓	↓	↓	↓	↓	↓
GS	NA	↓	NA	NA	↓	NA	NA	NA
S100β	↓	↓	↓	↓	↓	↓	↓	↓
CX43	NA	NA	NA	NA	↓	NA	NA	NA
Aldh1l1 eGFP	↓	↓	↓	↓	↓	↓	↓	↓
GCaMP5G	↓	NA	↓	NA	↓	NA	NA	NA
IRES tdTomato	↑	↑	↑	NA	↑	NA	NA	NA
Aldh1l1 tdTomato	NA	NA	NA	NA	↑	NA	NA	NA

Table 2: *List of astrocytic proteins and the changes in protein expression observed in immunohistochemistry in response to mTBI. Red arrows represent downregulation and green arrows represent upregulation of proteins at different timepoints. hpi: hours post-injury. dpi: days post-injury. N/A: not applicable. Source: (Shandra et al., 2019)*

2 Materials and Methods

2.1 Mice

C57BL/6 mice, 9 of 14 weeks of age, of both sexes were used for weight drop injuries, since no sex-specific differences in mortality rates, righting reflex recovery time, or area covered by atypical astrocytes after mTBI were observed in our previous study (Shandra et al., 2019). Mice of both sexes were used in EC ablation experiments at 8 weeks of age. All animal procedures were approved by and conducted according to the guidelines of the Institutional Animal Care and Use Committee of Virginia Polytechnic and State University and were done in compliance with the National Institute of Health's Guide for the Care and Use of Laboratory Animals.

2.1.1 Mouse strains

For endothelial cell-specific ablation experiments, Gt(ROSA)26Sor$^{tm1(DTA)Jpmb}$/J mice (Jackson Laboratory stock #006331) were crossed with Tg(Cdh5-cre/ERT2)1Rha (MGI:3848982). We refer to Gt(ROSA)26Sor$^{tm1(DTA)Jpmb}$/J mice that express the diphtheria toxin A (DTA) subunit heterogeneously as DTA$^{(fl/wt)}$ mice and Tg(Cdh5-cre/ERT2)1Rha that express the transgene heterozygously as Cdh5(PAC)-CreERT2$^{tg/wt}$. In mTBI experiments, C57BL/6 mice were used, unless otherwise specified. Mice were purchased from The Jackson Laboratory and bred in-house.

2.1.2 Weight-drop

An impact acceleration weight drop TBI model was used to mimic mTBI without focal injury as previously described (Marmarou et al., 1994; Shandra et al., 2019). Mice were anesthetized with 3% isoflurane for 5 minutes, administered analgesic buprenorphine (0.05-0.1 mg/kg), then placed on a form pad. A flat steel disc was placed on the mouse's head to diffuse the impact across the cranium. A 100 g weight guided by a plexiglass tube was dropped from a 50 cm height. For the 10 and 30 minutes post injury (mpi) timepoints, a single injury was performed (1xTBI). For all other timepoints that occurred days post injury (dpi), the impacts were repeated (3 total) and occurred at a 45-minute inter-injury interval (3xTBI). Shams

underwent all procedures with exception of the weight drop.

2.1.3 Two-photon microscopy

Aldhl1l-eGFP/FB Adlh-1l1-eGFP//FVB/N mice were used for repeated *in vivo* two-photon imaging via a thinned-skull cranial window as described previously (Shandra & Robel, 2019; Shandra et al., 2019). First, mice were anesthetized with 3% isoflurane gas in an induction chamber and administered buprenorphine (0.1 mg/kg) rimadyl/carprofen subcutaneously (5 mg/kg). During the surgery, the animal's head was fixed in a stereotactic apparatus and the body temperature was maintained at 37.0°C. The level of anesthesia was maintained at 1.5–2% isoflurane gas. An eye lubricant was applied to the eyes of the animal to prevent corneal desiccation. A 2 cm circular area of the skull over the ROI was shaved using a hand drill. The ROI was thinned to ~50 μm thickness. Dental cement was used to cover the area around the ROI and to create a well. Mice were placed into a warm cage with hydrogel and moistened food to recover. Next, baseline images were acquired using a four-channel multiphoton laser scanning fluorescence microscope (Olympus FV1000MPE) equipped with an XLPLN25X/1.05 numerical aperture (NA) water-immersion objective (Olympus). After the baseline imaging session, mice were allowed to recover for one hour. After the recovery period, mice were anesthetized with 3% isoflurane gas in an induction chamber for five minutes and underwent removal of the dental cement cap. A metal disc was then placed over the exposed skull, and mTBI was induced three times with 45 min intervals between impacts. After the final impact, mice were placed in the stereotactic apparatus to apply cyanoacrylate glue and cover the ROI with a cover glass thereby installing a permanent window for long-term reimaging. During the imaging window installation, mice were kept at 1.5–2% isoflurane gas level. Dental cement was applied to create a well and cover the area around the thinned ROI. The control mice underwent only thinned skull preparation surgery, cover glass implantation, and imaging (Shandra et al., 2019).

2.1.4 Experimental design for endothelial cell (EC) ablation

DTA blocks protein synthesis, thus inducing apoptosis in the Cre-expressing cells (Ivanova et al., 2005). $DTA^{fl/wt}$ (fl: floxed allele, encoding loxP sites; wt: wild-type allele) mice express DTA under the Rosa26 promoter behind a stop cassette flanked by loxP sites, which interferes with DTA expression until the stop cassette is removed by Cre recombinase. Cre recombinase is fused with an estrogen receptor and expressed behind the Cdh5(PAC) promoter and as part of a complex in Cdh5(PAC)-$CreERT^{tg/wt}$ mice (tg: allele carries transgene; wt: wild-type allele). This restricts expression to ECs and enables the timed relocalization of the CreERT protein complex to the nucleus for excision of the stop cassette only after tamoxifen (TX) administration. Cdh5(PAC)-$CreERT^{tg/wt}$ is expressed and causes Cre-mediated recombination in a sparse number of endothelial cells.

Experimental $DTA^{fl/wt}$// Cdh5(PAC)-$CreERT^{tg/wt}$ mice were given a single dose of Tx. Control $DTA^{fl/wt}$// Cdh5(PAC)-$CreERT^{tg/wt}$ mice were given a corn oil solution, and mice that expressed either $DTA^{wt/wt}$// Cdh5(PAC)-$CreERT^{tg/wt}$ or $DTA^{fl/wt}$// Cdh5(PAC)-$CreERT^{wt/wt}$ were given a single dose of Tx. There were no differences between the control groups, so data were pooled for analysis.

2.1.5 Tamoxifen administration

To drive Cre expression in adult mice, Tx (Sigma, catalog #T6548) was dissolved at 10 mg/mL in 100% corn oil (Sigma, catalog #C2867) for 2 hours while shaking at 37°C. The Tx solution was administered once via oral gavage at 330 mg/kg once.

2.1.6 Cadaverine/dextran administration

To assess blood-brain barrier integrity, Alexa Fluor-555 Cadaverine (950 Da, 1mg; Invitrogen, Catalog #A30677) or Dextran conjugated to Tetramethylrhodamine (70 kDa, 25 mg; Invitrogen, Catalog #D1818) was injected into the mouse retro-orbital sinus. Cadaverine (1 mg) or Dextran (25 mg) was dissolved in 300 uL of sterile saline. Each mouse was injected with a volume of 100 uL (0.33 mg for Cadaverine or 8.33 mg for Dextran). Mice were perfused

transcardially with phospho-buffer saline (PBS) followed by 4% paraformaldehyde (PFA) 30 minutes after Cadaverine injection.

2.2 Histology

Brains were harvested after transcardial perfusion and post-fixed in 4% PFA overnight. Coronal slices were cut at 50 μm thickness using a vibratome (Campden 5100mz). IHC was performed using the primary antibodies in PBS with 10% goat serum and 0.5% Triton X-100 at 4°C overnight. Slices were washed in PBS and incubated in secondary antibody solution of PBS with 10% goat serum and 0.5% Triton X-100 for 1-2 hours at room temperature. Then, 4,6-diamidino-2-phenylindole (DAPI) was included in a secondary antibody solution as needed. Slices were washed in PBS three times for 10 minutes each and then mounted onto glass microscope slides with Aqua-Poly/Mount (Polysciences, catalog #18606).

2.3 Primary astrocyte cell culture

Before performing primary astrocyte cell culture experiments, 12 mm and 8 mm coverslips were placed in 24 and 48-well plates respectively and were incubated in poly-o-orithinine for 2-24 hours in the biosafety cabinet. Coverslips were washed with autoclaved Millipore water 3 times. Next, 10 μg/mL of laminin in 1x filtered PBS were added to the coverslips and incubated overnight. Laminin solution was pipette back in the falcon tube and can be reused for up to 4 weeks.

Five C57BL/6 P3-P5 mouse pups were decapitated, and cortices were dissected in carbogenated (95% O_2/5% CO_2) artificial cerebrospinal fluid (ACSF: 125 mM NaCl, 3 mM KCl, 1.25 mM NaH_2PO_4 25 mM $NaHCO_3$ 25 mM glucose). Brain cortices were minced and digested via a Papain Dissociation kit (Worthington Biomedical) and placed in a 37°C hot water bath for 10-15 minutes. Then, the tissue was titruated by using a serological pipette and placed in the centrifuge at 300*rcf for 5 minutes at room temperature. Next, the supernatant was discarded, and 1 mL of resuspension media was added to the tissue. The tissue was titruated with a fire-polished pipette 5-7 times. The remaining 2 mL of resuspension media was added to the tissue

homogenate. After titruating the tissue homogenate in resuspension meeting, it was layered on top of 5 mL of albumin-ovomucoid inhibitor in a separate Falcon tube. Next, the solution was centrifuged at 300*rcf for 3 minutes at room temperature. The supernatant was discarded and 4 mL of 0.5% bovine serum albumin (BSA) in PBS was added to the tissue. Then, 1 mL of 0.5% BSA in PBS was added to a 70 μm BD Falcon filter, and the tissue homogenate was added to the filter to remove excess tissue that was not fully digested.

The filtered solution was centrifuged at 300*rcf for 3 minutes at 4°C. Then, 150 μL of 0.5% BSA in PBS was added to the pellet, and magnetic microbeads containing antibodies that attach to the cell of interest were added to the minced tissue. More specifically, 30 μL of both Cd11 (which binds to microglia) and myelin (which binds to NG2 cells) microbeads were added to the tissue. Next, the solution is placed in the fridge to incubate at 4°C for 10 minutes. After incubation, 1 mL of 0.5% BSA in PBS is added to the tissue, and the tissue was centrifuged at 300*rcf for 3 minutes at 4°C to remove excess microbeads. Next, the supernatant was discarded, and 500 μL was added to the pellet. Then, the tissue was added to the LS columns to allow the astrocytes and neurons to be collected in the falcon tube through a process called magnetic-activated cell sorting (MACS). The LS column containing the microglia and NG2 cells was discarded, and the flow-through was centrifuged at 300*rcf for 3 minutes at 4°C. The supernatant was discarded and 150 μL of 0.5% BSA in PBS was added to the pellet. Then, 20 μL of FcR blocking solution was added to the astrocyte/neuron pellet and placed in the fridge at 4 °C for 10 minutes. Then, 20 μL of astrocyte cell-specific antibody-2 (ACSA-2) microbeads (which binds to astrocytes) were added to the pellet and placed in the fridge to incubate at 4 °C for 10 minutes. After incubation, 1 mL of 0.5% BSA in PBS is added to the tissue, and the tissue was centrifuged at 300*rcf for 3 minutes at 4°C to remove excess microbeads. Next, the supernatant was discarded, and 500 μL was added to the pellet. Then, the tissue was added to the LS columns to allow the neurons to be collected in the falcon tube. The neurons were discarded and 5 mL of 0.5% BSA in PBS was added to the LS column. Astrocytes were eluted from the LS

column with a supplied plunger into a separate falcon tube. The astrocytes were centrifuged at 300*rcf for 5 minutes at 4°C (Holt, Stoyanof, & Olsen, 2019). Then, 50x B27 stock solution was diluted to 5x in serum-free astrocyte media (0.5x Neurobasil Media (NBM), 0.5x Minimum Essential Media (MEM), 1 mM sodium pyruvate, 1 mM glutamine, 500 U penicillin/streptomycin). Then, the supernatant was removed, and 1 mL of 5x B27 serum-free media was added to the astrocyte pellet. The number of astrocytes was counted with a hemocytometer to determine the cell density required to perform *in vitro* experiments.

On 12 mm coverslips, 375 µL of 5x B27 serum-free media and primary astrocytes were added to each well on the day of the MACS isolation. Astrocytes were supplemented to 500 µL with fresh B27 serum-free media on day 1 post-isolation followed by a complete replacement of the media on day 3 post-isolation. Every 3 to 4 days, the wells were replaced with half the volume of fresh 5x B27 media to maintain the cell cultures before treatment.

On 8 mm coverslips, 175 µL of 5x B27 serum-free media and primary astrocytes were added to each well on the day of the MACS isolation. Astrocytes were supplemented to 250 µL with fresh B27 serum-free media on day 1 post-isolation followed by a complete replacement of the media on day 3 post-isolation. Every 3 to 4 days, wells were replaced with half the volume of fresh 5x B27 media to maintain the cell cultures before treatment.

2.3.1 Cardiac puncture

Adult male C57B/6. mice were anesthetized with 3% isoflurane for 5 min by using the SomnoSuite Small Animal Anesthesia System. A 25G needle was used to withdraw blood from the left ventricle and collected in a 1.5 mL Eppendorf tube (Parasuraman, Raveendran, & Kesavan, 2010). Blood was centrifuged at 14,000 rpm for 5 min at 4°C to separate erythrocytes and leukocytes contained in whole blood to isolate blood plasma.

2.3.2 Heat-denaturation

Heat-denaturation was performed by first aliquoting 60 µL of fresh mouse plasma in a separate Eppendorf tube. Then, the aliquot was heated with a Thermomixer at 75°C for 5

minutes. Heat-denatured plasma was diluted to 600 µL with 5x B27 serum-free astrocyte media and thoroughly mixed before treating the coverslips in 48 well-plates for 24 hours.

2.3.3 Treatment of blood-borne factors *in vitro*

Fresh mouse plasma or heat-denatured plasma was diluted to 10% in 5X B27 serum-free media and was added to the primary astrocyte cultures for 24 hours in the incubator. Albumin and fibrinogen were first diluted to 10 g/dL and 70 g/dL in autoclaved Millipore water, respectively. Then, the proteins were diluted to 4.5 g/dL and 400 mg/dL, respectively in 5x B27 serum-free media and added to the primary astrocyte cultures for 24 hours in the incubator.

2.4 Immunocytochemistry

Primary astrocyte cultures were washed three times with 1x PBS and then fixed in 4% PFA for 15-20 minutes. Coverslips were washed again three times with 1x PBS make both primary and secondary antibody solutions, refer to Material and **Methods 2.2**. Coverslips were treated with primary antibody solution at 4C for a minimum of 2 hours. Then, they were washed three times with 1x PBS, before treating them with secondary antibody solution at room temperature for 1-2 hours. Coverslips were mounted onto glass microscope slides with Aqua-Poly/Mount (Polysciences, catalog #18606).

2.5 Data analysis

2.5.1 Quantification of Glt1 Loss

Large image scans of brain slices were taken by using a 20x objective with three to five slices used per animal. Regions of interest (ROIs) were drawn in Glt1 negative areas in the cortex, excluding neurons and large blood vessels that also show up as Glt1 negative via ImageJ. Loss of Glt1 was reported as a percentage area of the total cortex lacking Glt1 in each slice. The values were reported by plotting data by animal, in which the percentage represents the total area lacking Glt1 in the cortex.

2.5.2 Quantification of Cadaverine Leakage

Large image scans of brain slices were taken by using a 10x objective with five slices used

per animal. ROIs containing Cadaverine leakage were drawn in ImageJ based on three criteria: 1) Cadaverine+ cells appeared brighter than background signal, 2) Cadaverine+ cells were clustered close to each other, and 3) there were at least 10 Cadaverine cells contained in each drawn ROI. Cadaverine leakage was reported as percentage leakage area in the cortex per slice. The values were reported by plotting the data points by animal, in which the percentage represents the total area containing Cadaverine leakage in the cortex.

2.5.3 Quantification of ZO-1

Zonula occludens (ZO-1) vessel coverage was quantified by imaging areas containing Glt1 loss and BBB leakage. Then, ZO-1 images were converted to binary images based on intensity and size on ImageJ. The resulting binary masks were overlaid onto corresponding images of the blood vessel marker CD31. A CD31+ blood vessel was outlined in ImageJ, which generated a plot profile that reported the number of pixels that either include or do not include ZO-1. The number of pixels containing ZO-1 was normalized by the total number of pixels contained in the ROI.

ZO-1 signal intensity levels were quantified by drawing freehand selections in ImageJ around areas containing Glt1 loss and measuring the average grayscale value in selected ROIs. Similar areas were selected in shams. Three confocal images were taken in three different slices per mouse, and data points were plotted by animal.

2.5.4 Quantification of GLUT1

Glucose transporter-1 (GLUT1) signal intensity levels were quantified by drawing freehand selections in ImageJ around areas containing Glt1 loss and measuring the average grayscale value in selected ROIs, as described in the previous section. Similar areas were selected in shams. Three confocal images were taken in three different slices per animal, and data points were plotted by animal.

2.5.5 Quantification of Glt1/Kir4.1 *in vitro*

Six ROIs were taken per coverslip by using a 40x objective and immersion oil placed on

the coverslips. Images were collapsed into a maximum intensity projection on ImageJ with three z-stacks used for each maximum-intensity projection. Then, the average grayscale value was measured for both the Glt1 and Kir4.1 channels. Next, the area coverage of both proteins was quantified by binarizing both channels to select cells that express either Glt1 or Kir4.1. Lastly, the average grayscale value was divided by the area coverage of both proteins, and values were normalized with respect to the control coverslips. Data points were color-coded with respect to the independent culture and were plotted by either ROI or coverslip, depending on the number of independent cultures used in each experiment.

2.5.6 Quantification of CD45+ cells in the cortex

Brain slices were stained for CD45, which labels peripheral immune cells, such as monocytes and leukocytes. The number of CD45+ cells present in the cortex (excluding the meninges) was quantified by scanning through the eyeport and counting individual cells with a hand-held manual counter. Three brain slices per mouse were used, and the square root of the sum of all CD45+ cells per mouse was calculated. The data points were reported by mouse.

2.5.7 Quantification of area coverage of CD31+ blood vessels

Images of four ROIs were taken in the cortex (two images of the opposing lateral regions and two opposing regions towards the medial line) with a 20x objective. Three slices per mouse were used in the quantifications. Pixels containing CD31+ signal were selected by thresholding and binarizing the images via ImageJ. Then, the area coverage of CD31+ blood vessels in each ROI were quantified. To estimate the number of ECs ablated after Tx administration, data were normalized with respect to the control for the three timepoints used. Data points were plotted by mouse.

2.5.8 Quantification of β-dystroglycan

β-dystroglycan (bDG) signal intensity levels were quantified by drawing freehand selections in ImageJ around areas containing Glt1 loss and measuring the average grayscale value in selected ROIs, as described in the previous sections. Similar areas were selected in

shams. Three confocal images were taken in three different slices per mouse, and data points were plotted by mouse.

2.5.9 Quantification of AQP4

Aquaporin-4 (AQP4) signal intensity levels were quantified by drawing freehand selections in ImageJ around areas containing Glt1 loss and measuring the average grayscale value in selected ROIs, as described in previous sections. Similar areas were selected in shams. Three confocal images were taken in three different slices per mouse, and data points were plotted by mouse.

2.5.10 Quantification of MMP9

Matrix metalloproteinase-9 (MMP9) signal intensity levels were quantified by drawing freehand selections in ImageJ around areas containing Glt1 loss and measuring the average grayscale value in selected ROIs, as mentioned in previous sections. Similar areas were selected in shams. Three confocal images were taken in three different slices per mouse, and data points were plotted by mouse.

2.5.11 Quantification of pSMAD2

pSMAD2 signal intensity levels were quantified by drawing freehand selections in ImageJ around areas containing Glt1 loss and measuring the average grayscale value in selected ROIs, as mentioned in previous sections. Similar areas were selected in shams. Three confocal images were taken in three different slices per mouse, and data points were plotted by ROIs and are color-coded by mouse.

2.6 Statistics

2.6.1 For All Data Sets

Statistics were calculated and graphed using GraphPad Prism 8 (GraphPad Software). All data were tested for Gaussian distribution using the Kolmogorov–Smirnov (KS) normality test. Statistical tests were chosen accordingly and are specified in the results section or figure legend. For all graphs, data points were plotted as the number of mice or coverslips in

scatterplots and mean with standard error of the mean (SEM). Data points from the same mouse or culture were plotted as dots of the same color. Statistics were also run after averaging per mouse, and p values differed but with no overall change in significant group differences. Statistical significance is indicated by *p≤0.05, **p≤ 0.01, ***p≤ 0.001, **** p≤ 0.0001.

2.6.2 Poisson Distribution for CD45+ data

Quantification of CD45+ cells fall under a Poisson distribution instead of the standard Gaussian distribution because the number of CD45+ cells is reported as discrete data. To normalize and stabilize the variance of the data, the square root of the total number of CD45+ cells per mouse was calculated, followed by either a one-factor or two-factor ANOVA to compare groups.

3 Results

3.1 Loss of astrocytic proteins correlates with long-term neurological consequences after mTBI

First, we explored how this atypical astrocyte response is relevant in the context of brain pathology after mTBI. One of the neurological consequences associated with mTBI is post-traumatic epilepsy (PTE), so I compared the presence of Glt1, which we use as a readout for the atypical astrocyte response, in the cortex of mice that either did or did not develop seizures after mTBI. Here, I found that the mice that developed PTE after mTBI had increased Glt1 loss in the cortex compared to mice that did not experience seizures after injury **(Fig. 1a,b)**. These findings suggest that the atypical astrocyte response is correlated with poor neurological outcomes after mTBI.

To determine the early biological events that induce the atypical astrocyte response after injury, mice were given retro-orbital injections of Cadaverine (~1 kDa) after mTBI to assess for BBB integrity. The presence of Cadaverine leakage in the brain indicates BBB damage. We found that areas of Cadaverine leakage overlapped with areas containing loss of the astrocytic markers, including Glt1, Kir4.1, S100β, and Aldh1l1-eGFP, suggesting that the BBB leakage may cause atypical astrocytes after mTBI **(Fig. 2)**.

Figure 1

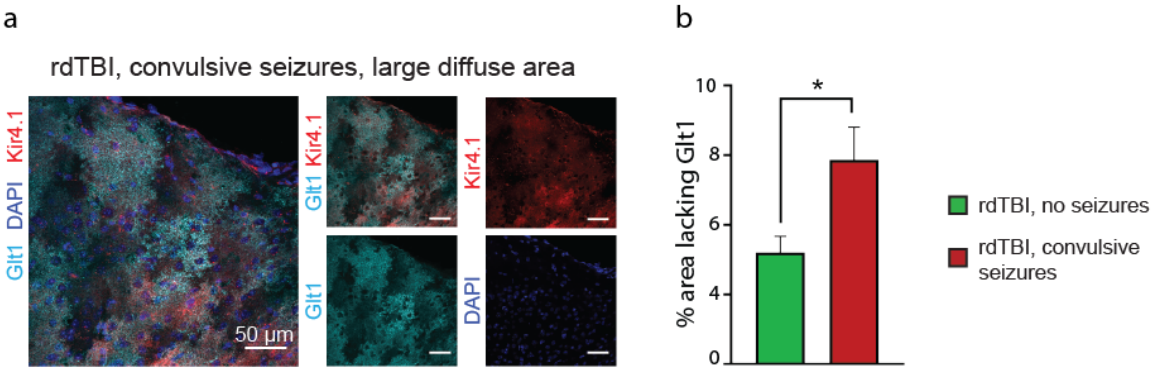

Figure 1: *Increased area containing atypical astrocytes is correlated with likelihood of developing PTE after mTBI.* ***a.*** *The cortex of mice that developed PTE after mTBI had more*

Glt1/Kir4.1 loss compared to mice that did not experience seizures after injury. ***b.*** *Percentage area containing Glt1 loss was quantified between mice that developed or did not develop PTE. (mice without PTE, 3.21 ± 0.4604, n=4. mice with PTE, 5.871 ± 0.9337, n=4. Unpaired t-test significant difference between rdTBI, no seizures and rdTBI seizures. rdTBI, no seizures vs. rdTBI, convulsive seizures, p=0.0432).*

Figure 2

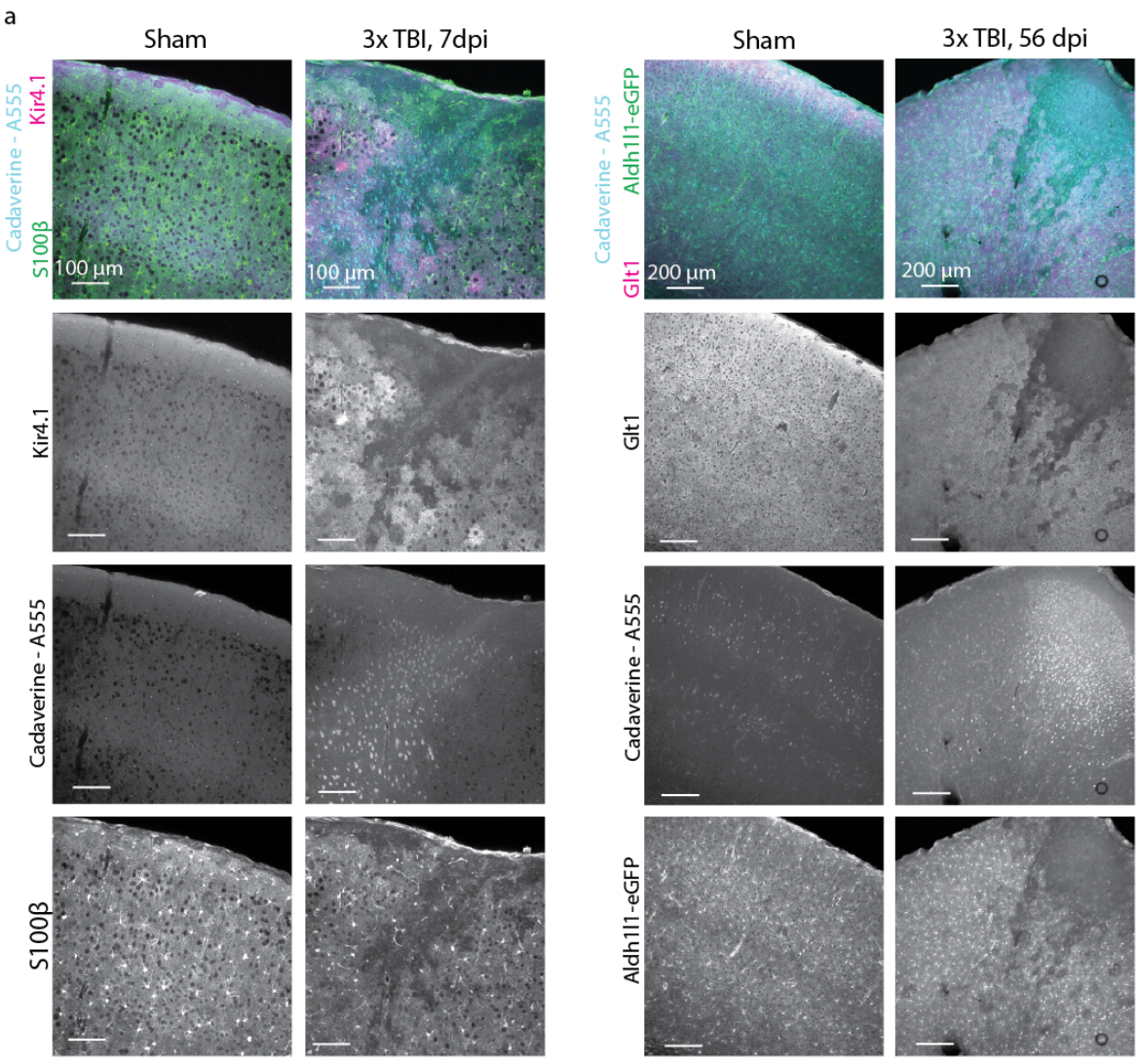

Figure 2: *BBB leakage overlaps with the loss of astrocytic markers, Glt-1, Kir4.1, S100β and Aldh1l1-eGFP. Retro-orbital injections of Cadaverine were administered to mice 30 minutes before perfusion to assess BBB integrity. Loss of Kir4.1 and S100β occurred at 7 dpi, and*

atypical astrocyte response and BBB leakage were sustained at 56 dpi

3.2 Significant BBB leakage, with minimal vessel rupture, occurs as early as 1 day after mTBI

To determine if mTBI leads to BBB damage, we injected Cadaverine (0.33 mg/uL) retro-orbitally in mice to assess BBB integrity after single and repeated mTBI (**Fig. 3b**). While we observed little to no Cadaverine leakage in sham brain slices, we observed Cadaverine leakage overlapping with areas of Glt1 loss as early as 10 mpi (**Fig. 3a**). We used Glt1 loss as a readout for the atypical astrocyte response, after demonstrating that BBB leakage overlapped with loss of other astrocytic-proteins, such as S100β, Kir4.1, and Aldh1l1-eGFP (**Fig. 2)**. Significant Cadaverine leakage occurred at 1 dpi after both a single and repeated mTBI **(Figure 3c)**. Here, we demonstrate that even a single mTBI induces BBB damage after 10 mpi and continues at 1 dpi.

To assess the severity of blood vessel damage after mTBI, we stained for fibrinogen (340 kDa), a clotting factor that coagulates near sites of vessel rupture while it halts bleeding. Due to fibrinogen's large size, we expected that increased fibrinogen leakage into the brain parenchyma suggests large vessel damage after mTBI. We examined 18 brain slices from six mice that were subjected to mTBI and found that sparse fibrinogen deposition occurred in five out of 18 brain slices in four mice, whereas Cadaverine leakage was found in almost all slices and in multiple areas (**Fig. 3d**). Next, we assessed direct damage to blood vessels by using two-photon imaging to identify areas of vessel rapture before and after mTBI. In only 1 of 10 ROIs (n=3), we observed vessel rupture after mTBI or leakage of 70 kDa Dextran coupled with Tetramethylrhodamine **(Fig. 4)**. In addition to using two-photon imaging of areas of vessel rupture, we labeled fixed brain slices for Ki67 to measure EC proliferation after mTBI, which is required to repair damaged blood vessels. While few Ki67+ cells were found in the shams, the difference in the number of Ki67+/CD31+ ECs (3/9 mice subjected to mTBI in 3/27 brain slices) was negligible after mTBI, suggesting that some vessel repair occurs after injury **(Fig. 3f).**

Figure 3

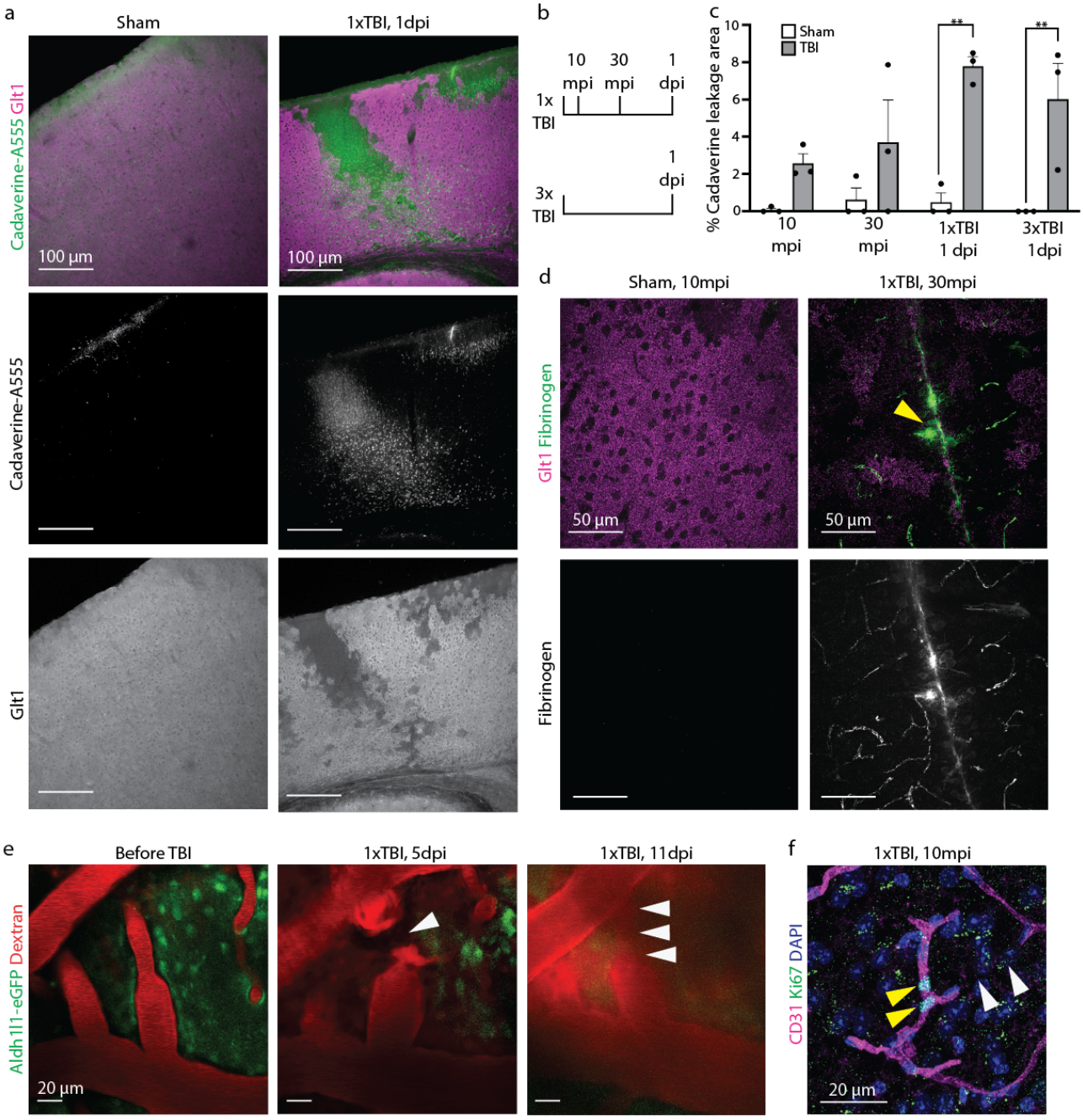

Figure 3: *Blood-brain barrier leakage occurs in areas of atypical astrocytes after mTBI.* ***a.*** *Cadaverine leakage occurred in the cortex within 10 minutes after a single mTBI and overlapped with regions of atypical astrocytes, as indicated by lack of expression of the glutamate transporter Glt1.* ***b.*** *Cadaverine was injected 30 minutes before perfusion for each timepoint. Single (1xTBI) and/or repeated (3xTBI) mTBIs were induced at the timepoints 10*

mpi, 30 mpi, and 1 dpi. ***c.*** *Cadaverine leakage was quantified as the percent area of total cortex and plotted by animal. For 1dpi, both 1xTBI and 3xTBI were examined. Data points are plotted by animal. (1x Sham 10mpi, 0.0864 ± 0.0834, n= 3;1xTBI 10mpi, 2.5886 ± 0.4985, n= 3; Sham 30mpi, 0.6329 ± 0.6329 1xTBI 30mpi, 3.6953 ± 2.2832, n= 3; 1x Sham 1dpi; 0.4930 ± 0.4930 1xTBI 1dpi, 9.072 ± 2.086, n=3; 3x Sham 1dpi, 0 ± 0;3xTBI 1dpi, 6.0253 ± 1.9186, n= 3. Two-way ANOVA significant for post-injury timepoint, p< 0.0001; Sidak's multiple comparisons test. Sham vs. 1xTBI 10mpi, p=0.4375; Sham vs. 1xTBI 30mpi, p=0.2560; Sham vs. 1xTBI 1dpi, p= 0.0012; Sham vs. 3xTBI 1dpi, p= 0.0063).* ***d.*** *Few areas of fibrinogen deposition (yellow arrowhead), were found in regions of atypical astrocytes, as indicated by lack of Glt1 expression.* ***e.*** *Live imaging of Dextran-labeled vessels using two-photon microscopy revealed vessel rupture (white arrowheads) and reduced perfusion at 5 dpi. Reperfusion and repair of the same vessel (multiple white arrowheads) was observed at 11 dpi.* ***f.*** *The cell cycle marker Ki67 colocalized with the vessel marker CD31 (yellow arrowheads) in areas of abruptly short vessels (white arrowheads), which indicated vessel proliferation. Of the 9 mice and 27 slices examined after mTBI, only 3 mice and 3 slices (one slice in each mouse) showed $Ki67^{+}/CD31^{+}$ colocalization. For 9 sham mice and 12 slices examined, no colocalization was detected. mpi = minutes post injury, dpi = days post injury.*

Figure 4

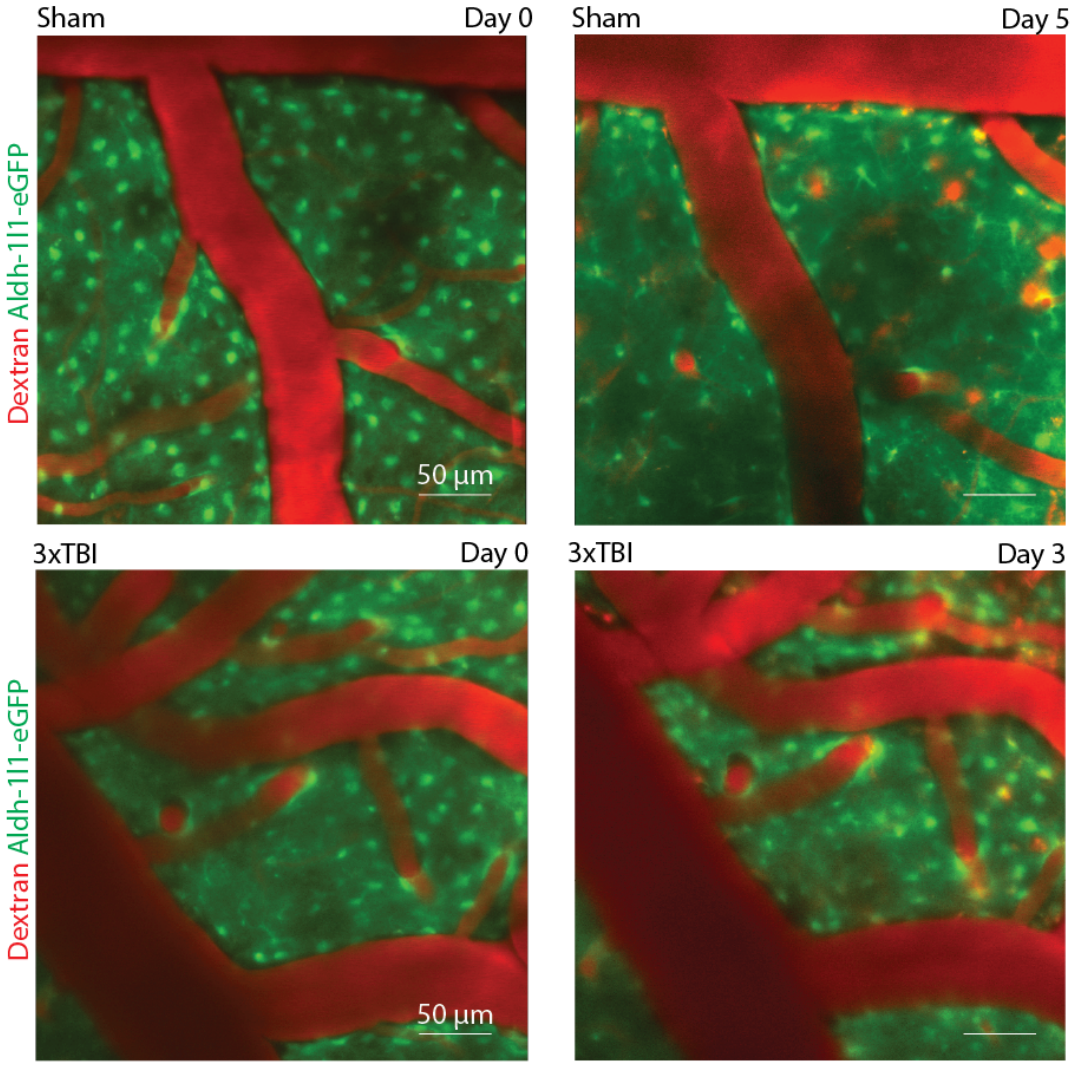

Figure 4: *mTBI does not cause significant vessel rupture. Intact blood vessels after mTBI in 9 out of 10 ROIs. Live imaging of the cerebral vasculature after retro-orbital injection of a 70 kDa Dextran coupled to Tetramethylrhodamine using two-photon microscopy reveals intact vasculature and perfusion at all timepoints (n=3, 9 ROIs total, 3 mice were imaged before and acutely after repeated TBI, 2 out of 3 mice were subsequently imaged vessel). The figure depicts the final timepoint (3dpi). No leakage of the Dextran was observed in the shams until day 5 (n=1, 3 ROIs).*

3.3 mTBI triggers the loss of proteins responsible for maintaining BBB properties

Since little to no vessel rupture was observed, we want to determine if the increased BBB damage after mTBI was due to impaired BBB properties. First, we assess the expression and amount of blood vessel coverage of zonula occludens-1 (ZO-1), a protein involved in forming tight junctions in the BBB, which are important for preventing pathogens and blood-borne factors from entering the brain parenchyma. In the shams, CD31+ blood vessels contain continuously labeled ZO-1, while ZO-1 vessel coverage and expression are reduced significantly in areas with Cadaverine leakage and atypical astrocytes in the cortex, as early as 10 mpi (**Fig. 5a-c)**. Together, these data suggest that mTBI causes BBB damage by disrupting vessel coverage and reducing ZO-1 expression.

Another BBB property that we want to examine was its metabolic barrier, which contains transporters that shuttle water and nutrients into the brain. To determine if mTBI affects the metabolic component of the BBB, we assess for EC-specific expression of GLUT1, which accounts for 90% of all glucose transporters in the brain (Pardridge, Boado, & Farrell, 1990) In the shams, large blood vessels were labeled with GLUT1, while GLUT1 fluorescence intensity was reduced at 1 dpi in areas containing atypical astrocytes and Cadaverine leakage (**Fig. 5d, e)**. Thus, in addition to showing that ZO-1 expression and vessel coverage are reduced after mTBI, we demonstrated that mTBI triggers disruption of the BBB's metabolic properties.

Figure 5

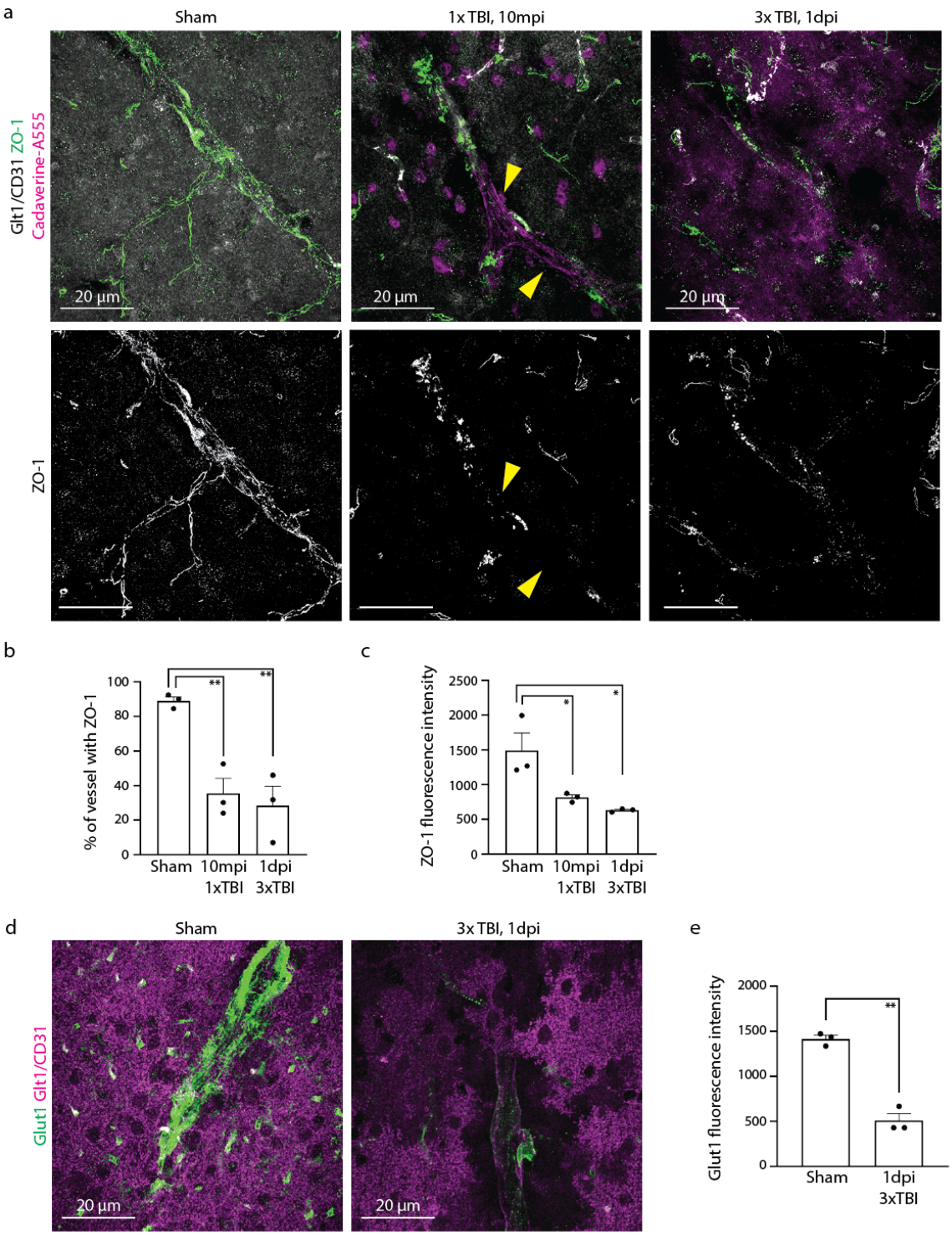

Figure 5: *The blood-brain barrier is damaged after mTBI.* ***a.*** *Labeling of the tight junction protein ZO-1 was reduced and discontinuous after single and repeated mTBI, occurring in areas of atypical astrocytes (indicated by lack of Glt1 expression) and Cadaverine leakage.*

Some vessels completely lacked ZO-1 labeling (yellow arrowheads). ***b.*** *Continuity in ZO-1 labeling of vessels was quantified by binarizing ZO-1 signal and drawing a line along the vessel using the vessel marker CD31 as a guide. The percentage of pixels with ZO-1 was calculated as the percent of vessels with ZO-1 and was plotted by animal. (Sham, 89.05 ± 2.301, n= 3; 1xTBI 10mpi, 35.65 ± 8.654, n= 3; 3xTBI 1dpi, 28.33 ± 11.40, n= 3. One-way ANOVA significant for post-injury timepoint, p= 0. 0041. Dunn's multiple comparisons test. Sham vs. 1xTBI 10mpi, p= 0. 0073; Sham vs. 3xTBI 1dpi, p= 0. 0039).* ***c.*** *Fluorescence intensity for the lines drawn in* ***b*** *were quantified and reported as mean grayscale (GS) units. (Sham, 1492 ± 251.6, n= 3; 1xTBI 10mpi, 814.7 ± 38.31, n= 3; 3xTBI 1dpi, 632.6 ± 14.37, n= 3; One-way ANOVA significant for post-injury timepoint, p0.0139. Tukey's multiple comparisons test. Sham vs. 1xTBI 10mpi, p=0.0398; Sham vs. 3xTBI 1 dpi, p=0.0145).* ***d.*** *The endothelial glucose transporter GLUT1 was greatly reduced in its labeling at vessels after mTBI in areas of atypical astrocytes indicated by lack of Glt1 expression.* ***e.*** *Fluorescence intensity of GLUT1 was quantified after mTBI and reported as mean grayscale units. Data points are plotted by animal. (Sham, 1416 ± 41.32, n= 3; 3xTBI 1dpi, 508.8 ± 79.17, n= 3; Mann-Whitney Test. Sham vs. 3xTBI 1 dpi, p=0.002).*

3.4 Leakage of blood-borne factors is sufficient to trigger atypical astrocytes

3.4.1 EC ablation reduces the expression of proteins involved in maintaining BBB properties and induces an atypical astrocytes response

Based on our observations of Cadaverine leakage overlapping with atypical astrocyte areas in the cortex, we hypothesize that the leakage of blood-borne factors triggers the atypical astrocyte response after mTBI. To determine if BBB leakage is sufficient to trigger atypical astrocytes in the absence of injury, we cross mice that express the Tx-inducible CreERT2 recombinase driven by the EC-specific Cadherin 5 PAC promoter (Cdh5(PAC)) with mice that express the DTA subunit behind a stop cassette flanked by loxP sites. A single low dose of Tx was administered to adult mice to trigger EC ablation, thus inducing BBB leakage.

After quantifying the area coverage of CD31+ after Tx administration, there are no significant changes compared to the controls, yet I observed Cadaverine leakage due to the DTA-mediated apoptosis (Ivanova et al., 2005) of ECs as early as 2 hours post-administration (hpa) of Tx (**Fig. 6a,b).** Here, we establish that a sparse ablation of ECs can induce significant BBB damage. Also, we observe increased entry of CD45+ cells at 6 hours after EC ablation, but number of CD45+ cells returns to levels similar to those of controls at 1 dpa **(Fig. 6c,d)**, showing that EC ablation does not lead to increased immune cell infiltration. I see a significant decrease in ZO-1 vessel coverage as early as 2 hpa **(Fig. 7a-c)**. However, the ZO-1 fluorescence intensity remains unaffected after EC ablation compared to the controls, suggesting a different mechanism of tight junction loss after mTBI where its fluorescence intensity was reduced **(Fig. 7a-c)**. Overall, these data suggest that ablating a small number of ECs can trigger loss of tight junction proteins, contributing to induced BBB leakage.

After assessing ZO-1 protein expression and CD31+ blood vessel coverage after EC ablation, we measure endothelial GLUT1 expression to determine if EC ablation affected the BBB's metabolic barrier. As expected, I observe a significant decrease in GLUT1 expression as early as 2 hpa, and this reduction was sustained throughout the later timepoints, suggesting that EC ablation triggers BBB leakage via loss of proteins involved in maintaining the metabolic barrier.

Lastly, we hypothesize that BBB leakage triggers the atypical astrocyte response after mTBI, so we measured the area of Glt1 loss in the cortex after EC ablation. We observed significant Glt1 loss occurring as early as 6 hpa **(Fig 7f-h)**. In addition to measuring Glt1 loss, we observed Kir4.1 downregulation at 1 day post administration (dpa) of Tx, suggesting that BBB leakage is sufficient to induce atypical astrocytes and is consistent with our findings after mTBI (Shandra et al., 2019). In contrast to our observations after mTBI, GFAP upregulation was found near sites of Glt1/Kir4.1 loss in the cortex after 1 dpa.

Figure 6

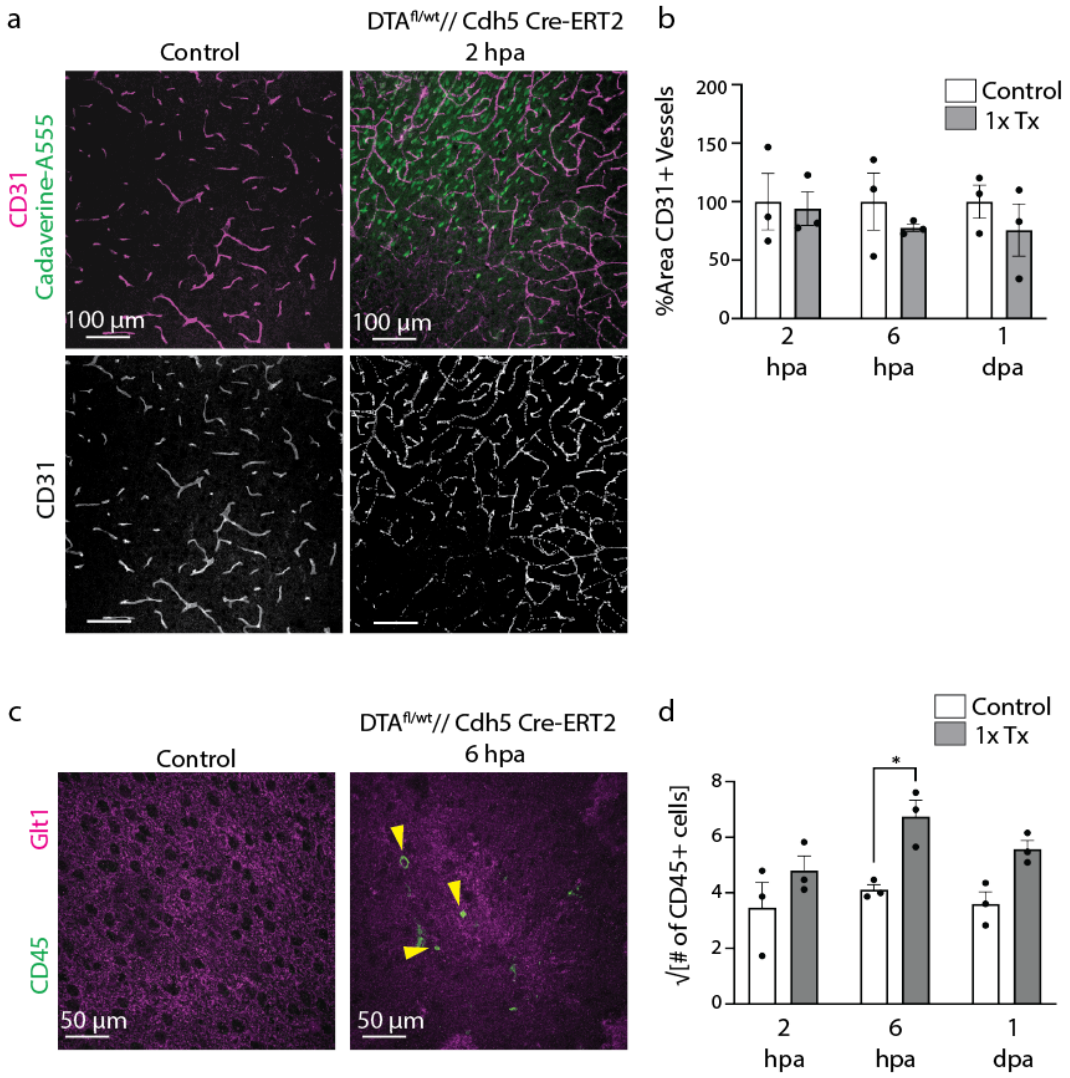

Figure 6: *EC ablation in the BBB is sparse after Tx administration.* ***a.*** *BBB leakage occurs at 2 hours after EC ablation despite minimal CD31 loss.* ***b.*** *Amount of EC loss after Tx administration was quantified by calculating average area coverage of CD31+ blood vessel. Data points are normalized in respect to control and are plotted by animal. (Control 2hpa, 100 ± 24.1136, n=3; Experimental 2hpa, 93.9849 ± 14.4379, n=3; Control 6hpa, 100 ± 24.4736, n=3; Experimental 6hpa, 77.6736 ± 3.3162, n=3; Control 1dpa, 100 ± 14.1257, n=3; Experimental 1dpa, 75.6227 ± 22.2295; Two-way ANOVA not significant for EC ablation, p=0.2717, and not significant for post-administration timepoint. p=0.8665. Sidak's multiple*

comparisons test. (Control 2hpa vs. Experimental 2hpa, p=0.9945; Control 6hpa vs. Experimental 2 hpa, p=0.7993; Control 1dpa vs. Experimental 1dpa, p=0.7550) ***c.*** *Number of CD45+ cells is increased at 6 hours after EC ablation but this returned to that of the controls at 1 dpa.* ***d.*** *Immune cell infiltration was quantified by taking the square root of the total number of $CD45^+$ cells per animal. (Control 2hpa, 3.4670 ± 0.9074, n=3; Experimental 2hpa, 4.8087 ± 0.5209, n=3; Control 6hpa, 4.1150 ± 0.1823, n=3; Experimental 6hpa, 6.7575 ± 0.5883, n=3; Control 1dpa, 3.5976 ± 0.4418, n=3; Experimental 1dpa, 5.5802 ± 0.3118, n=3; Two-way ANOVA significant for EC ablation, p=0.0007, but not significant for post-administration timepoints. P=0.5052. Sidak's multiple comparisons test. Control 2hpa vs. Experimental 2hpa, p=0.2827; Control 6hpa vs. Experimental 6hpa. p=0.0142; Control 1dpa vs. Experimental 1dpa, p=0.0690).*

Figure 7

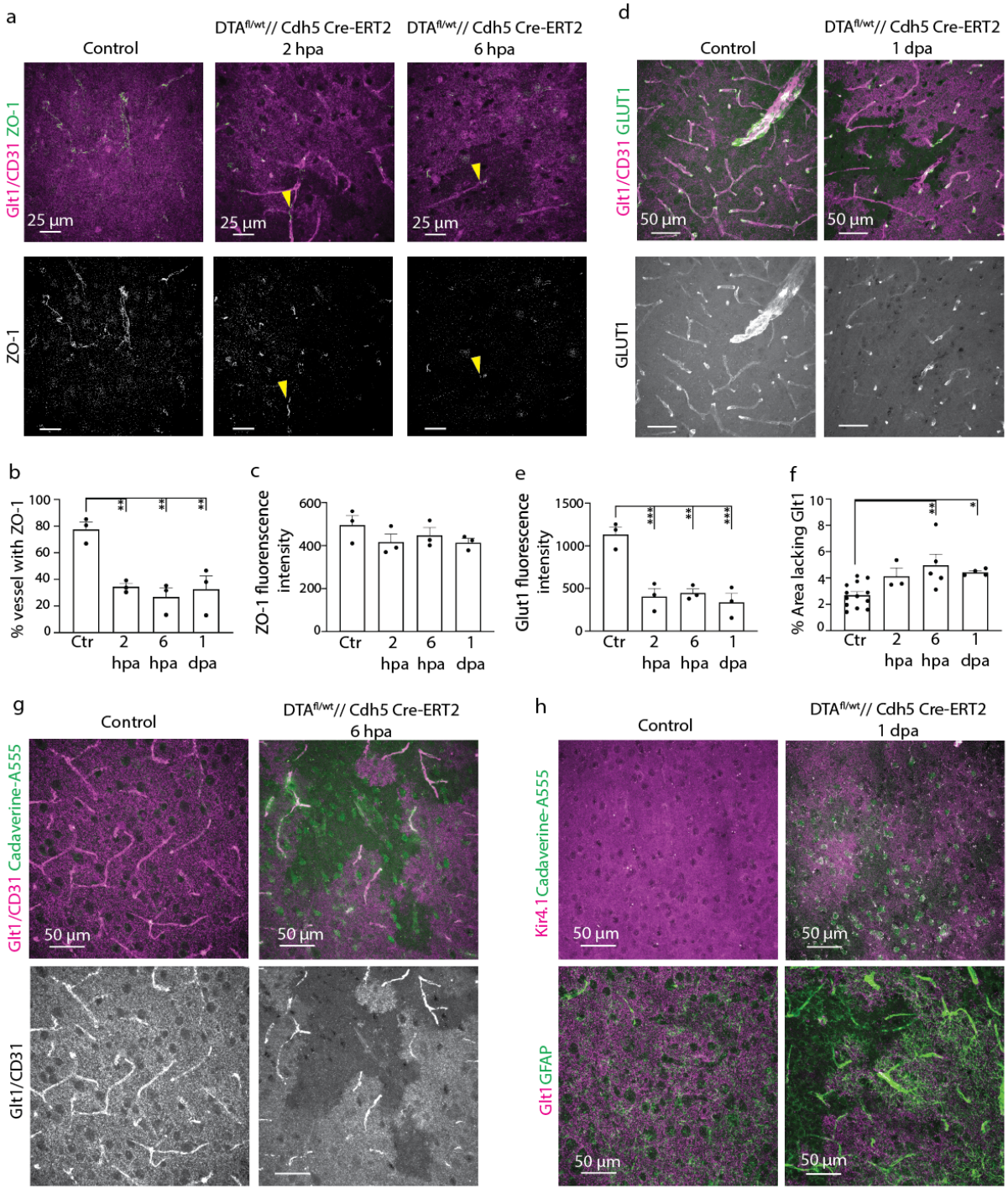

Figure 7: *BBB leakage induced via EC-specific genetic ablation is sufficient to trigger atypical astrocytes in the absence of mTBI.* ***a.*** *ZO-1 covering of CD31⁺ vessels was reduced as early as 2 hours after EC ablation and occurred in areas of atypical astrocytes, indicated by lack of Glt1*

expression (yellow arrowheads). ***b.*** *Continuity in ZO-1 labeling of vessels overlapping with atypical astrocytes was calculated as shown in* ***Figure 5b****. Data points are plotted by animal. (Control, 77.60 ± 5.497, n=3; 2hpa, 34.52 ± 2.570, n= 3; 6hpa, 26.82 ± 6.802, n= 3; 1dpa, 32.61 ± 10.08, n= 3. One-way ANOVA significant for post-administration timepoint. p= 0.0026. Dunnett's multiple comparisons tests. p<0.0001. Control vs. 2hpa, p= 0.0053; Control vs. 6hpa, p=0.0019; Control vs. 1dpa, p=0.0041).* ***c.*** *Fluorescence intensity for the ZO-1 lines drawn in* ***b*** *were reported as grayscale values. Data points are plotted by animal. (Control, 495.4 ± 44.22, n= 3; 2hpa, 417.1 ± 37.37, n= 3; 6hpa, 448.5 ± 35.16, n= 3, 1 dpa, 415 ± 19.10, n= 3. One-way ANOVA not significant for post-administration timepoint. p= 0.3907. Dunnett's multiple comparisons test. p=0.2543. Control vs. 2hpa, p=0.329; Control vs. 6hpa, p=0.681; Control vs. 1dpa, p=0.3118).* ***d.*** *GLUT1 labeling was reduced at vessels in atypical astrocyte areas lacking Glt1 after genetically ablating ECs after 2 hpa.* ***e.*** *Fluorescence intensity of GLUT1 in areas of atypical astrocytes was calculated and reported as grayscale values. Data points are plotted by animal. (Control, 1134 ± 88.85, n= 3; 2hpa, 404.1 ± 93.97, n= 3; 6hpa, 446.4 ± 47.41, n= 3; 1dpa, 338.5 ± 102.9, n= 3. One-way ANOVA significant for post-administration timepoint. p= 0.0006. Dunnett's multiple comparisons tests. p<0.0001. Control vs. 2hpa, p=0.0008; Control vs. 6hpa, p=0.0013; Control vs. 1dpa, p=0.0005).* ***f.*** *The percent area lacking Glt1 in the cortex was quantified per slice at 2 hours, 6 hours, and 1 day after EC ablation. Data points are plotted by animal. (Control, 2.703 ± 0.2573, n= 12; 2hpa, 4.139 ± 0.6135, n= 3; 6hpa, 4.960 ± 0.8508, n= 5 ; 1dpa, 4.436 ± 0.1246, n= 4. One-way ANOVA significant for post-administration timepoint. p= 0.004. Dunnett's multiple comparisons tests. p=0.0002. Control vs. 2hpa, p=0.1663; Control vs. 6hpa, p=0.0033; Control vs. 1dpa, p=0.0415).* ***g.*** *A decrease in Glt1 labeling occurred as early as 2hpa and overlapped with areas of Cadaverine leakage.* ***h.*** *Kir4.1 loss occurred in areas of atypical astrocytes (areas lacking Glt1), while GFAP boundary formation occurred in areas adjacent to atypical astrocytes at 1 dpa. hpa= hours post administration, dpa= days post administration*

3.5 Development of a serum-free culture system to test the effect of blood-borne factors

3.5.1 Plasma treatment triggers the atypical astrocyte phenotype *in vitro* at 24 hours

After establishing that BBB leakage is sufficient to cause atypical astrocytes, we want to screen for the specific blood-borne factors that cause the loss of astrocytic proteins. To overcome the challenges of identifying the causal link between each blood-borne factor and the atypical astrocyte response *in vivo*, I use a serum-free astrocyte cell culture assay. In previous *in vitro* studies, astrocytes were cultured in fetal bovine serum (FBS), which changed their morphology to resemble more immature cells (Holt & Olsen, 2016). Thus, we use a serum-free, chemically defined culture system to observe how primary astrocytes respond to different blood-borne factors.

First, I maintained primary astrocytes in serum-free media for 7 days *in vitro* (d*iv*) before treating them with 10% fresh mouse plasma for 2 hours and 24 hours. While there were no significant changes in Glt1/Kir4.1 expression after 2 hours of plasma treatment, expression of both proteins was reduced after 24 hours **(Fig. 8a-d)**. Here, I demonstrated that exposure to plasma-borne factors induces loss of Glt1/Kir4.1 expression *in vitro*, similar to what is observed *in vivo*.

Figure 8

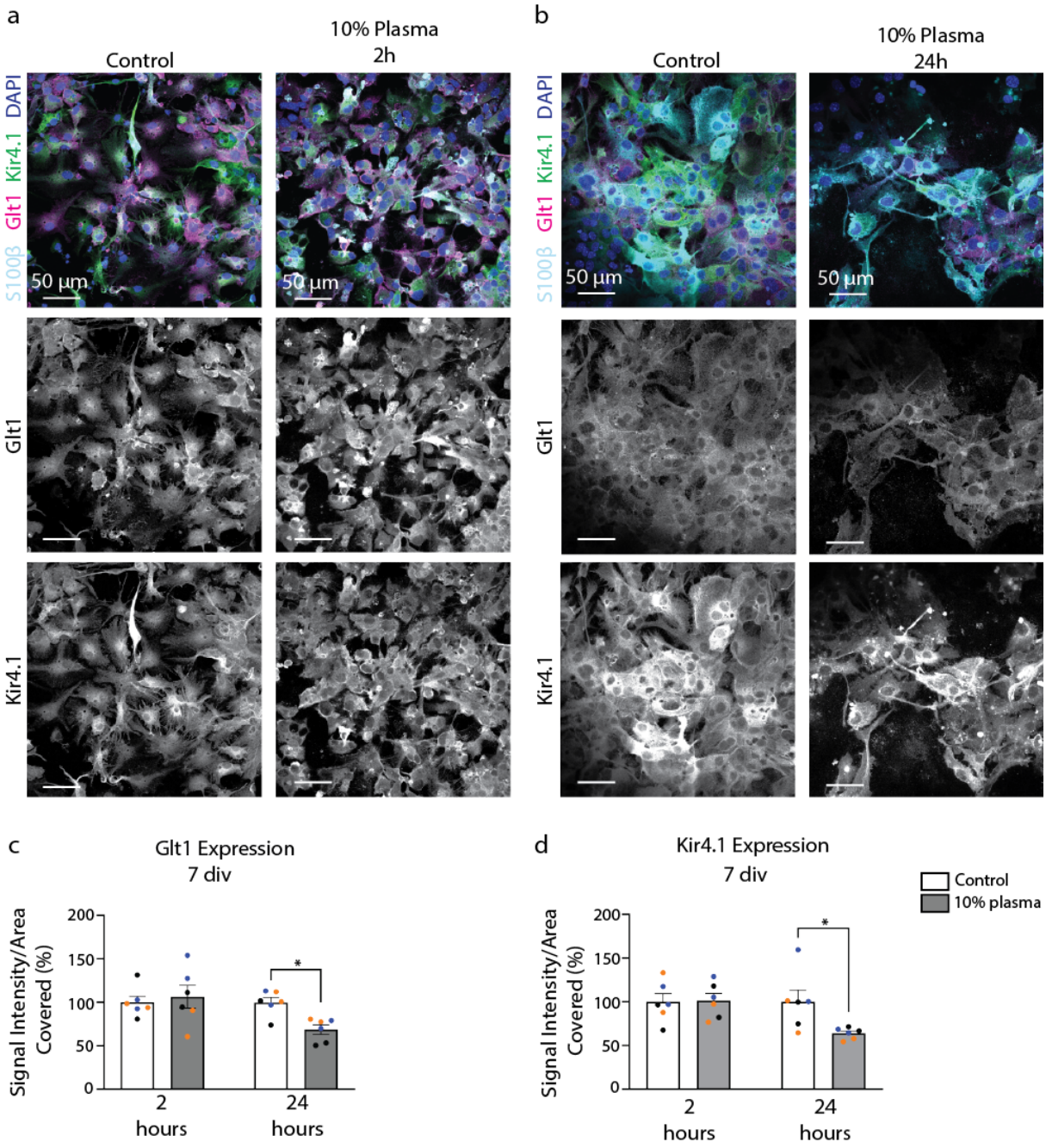

Figure 8: *Exposure to plasma triggered reduced Glt1/Kir4.1 expression after 24 hours in primary astrocytes maintained in serum-free media for 7 div.* ***a.*** *Glt1 and Kir4.1 expression remained unaffected after 2 hours of plasma exposure.* ***b.*** *A significant reduction in both Glt1 and Kir4.1 occurred at 24 hours.* ***c.,d.*** *Glt1 and Kir4.1 expression was quantified by dividing the mean grayscale value by the area coverage of each protein, then data were normalized*

with respect to the control group. Data points represent coverslips and are color-coded in respect to each independent culture. Three independent cultures were used in these experiments. (Glt1. Control 2 hours, 100.00 ± 7.00, n=6. Plasma 2 hours, 106.47 ± 13.18, n=6. Control 24 hours, 99.72 ± 5.81, n=6, Plasma 24 hours, 68.53 ± 5.48. Two-way ANOVA significant for treatment. P=0.0353. Sidak's multiple comparison tests. Control 2 hours vs. Plasma 2 hours, p=0.8357. Control 24 hours vs. Plasma 24 hours. p=0.0336. Kir4.1. Control 2 hours, 100.00 ± 9.37, n=6. Plasma 2 hours, 101.46 ± 8.25, n=6. Control 24 hours, 100.00 ± 13.48, n=6, Plasma 24 hours, 63.53 ± 2.67. Two-way ANOVA not significant for treatment. P=0.0564. Sidak's multiple comparison tests. Control 2 hours vs. Plasma 2 hours, p=0.9924. Control 24 hours vs. Plasma 24 hours. p=0.0244).

3.5.2 Treatment of primary astrocytes with plasma maintained on 12 mm and 8 mm coverslips

After establishing the conditions for the serum-free astrocyte culture, primary astrocyte cultures were initially incubated on 12 mm coverslips, Next, I downscaled the cell-culture assay by incubating primary astrocyte cultures on smaller coverslips to allow for more treatment conditions from one independent culture. I isolated primary astrocytes from two separate MACS isolations, plated them on 12 mm and 8 mm coverslips, incubated both cultures for 7 d*iv*, and treated both cultures with 10% fresh mouse plasma for 24 hours. On both coverslips, Glt1 and Kir4.1 signal intensity decreased after exposure to fresh plasma, allowing us to switch to using 8 mm coverslips to culture primary astrocytes to screen for more factors from one culture **(Fig. 9a-d)**.

Figure 9

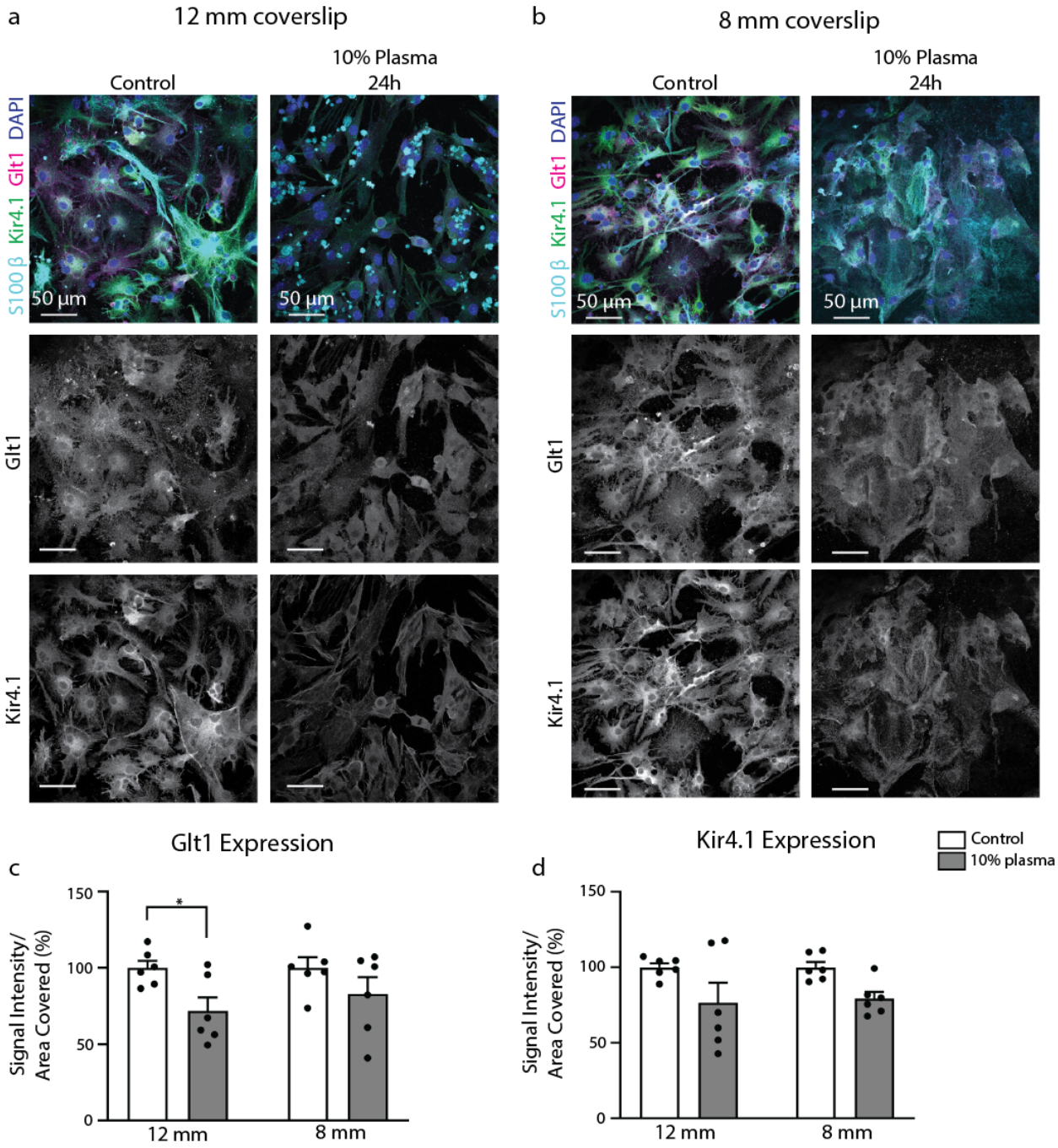

Figure 9: *Exposure to fresh mouse plasma causes reduction in Glt1/Kir4.1 in primary astrocyte cultures maintained in serum-free media for 7 div, regardless of coverslip size.* ***a.*** *Primary astrocytes incubating on 12 mm coverslips showed significant reduction of Glt1, but little reduction in Kir4.1 after plasma treatment.* ***b.*** *Plasma exposure triggered some loss of*

Glt1/Kir4.1 signal intensity in primary astrocytes maturing on 8 mm coverslips. ***c.,d.*** *Glt1 and Kir4.1 signal intensity was quantified by dividing the mean grayscale value by the area coverage of each protein, then data were normalized with respect to the control group. Data points are plotted by ROIs. One independent culture was used for these experiments. (Glt1. Control 12 mm coverslip, 100.00 ± 4.74, n=6. Plasma 12 mm coverslip, 71.67 ± 8.96, n=6. Control 8 mm coverslip, 100 ± 7.03, n=6, Plasma 8 mm coverslip, 82.90 ± 11.03. Two-way ANOVA not significant for treatment. p=0.5052. Sidak's multiple comparison tests. Control 12 mm coverslip vs. Plasma 12 mm coverslip, p=0.0494. Control 8 mm coverslip vs. Plasma 8 mm coverslip. p=0.2936. Kir4.1. Control 12 mm coverslip, 100.00 ± 2.72, n=6. Plasma 12 mm coverslip, 76.42 ± 13.34, n=6. Control 8 mm coverslip, 100.00 ± 3.61, n=6, Plasma 8 mm coverslip, 79.20 ± 4.57. Two-way ANOVA not significant for treatment. P=0.0564. Sidak's multiple comparison tests. Control 12 mm coverslip vs. 12 mm coverslip, p=0.0704. Control 8 mm coverslip vs. Plasma 8 mm coverslip. p=0.1180).*

3.5.3 Significant loss in Glt1/Kir4.1 expression in primary astrocytes maintained in media for 14 days at 24 hours

I next determined how maintaining primary astrocytes for different lengths of time *in vitro* affected their response to plasma exposure. Half of the wells were incubated for 7 d*iv*, while the remaining coverslips matured in media for 14 d*iv* before plasma treatment. First, I observed increased Glt1/Kir4.1 signal intensities in control primary astrocytes maintained in media for 14 d*iv* compared to the control astrocytes cultures for 7 d*iv*. Next, I compared the difference in Glt1/Kir4.1 signal intensities between the control groups and plasma treatment group for both astrocyte conditions. Here, I found that astrocytes maintained in media for 7 d*iv* and 14 d*iv* showed significant reduction in signal intensity for both proteins **(Fig. 10a-d)**. Also, increased Glt1/Kir4.1 signal intensity was observed in astrocytes maintained in media for 14 *div* compared to astrocytes maintained in media for 7 div in the absence of plasma. Therefore, these data highlight that astrocytes that are maintained in media for long periods of time are sensitive

to plasma exposure *in vitro*.

Figure 10

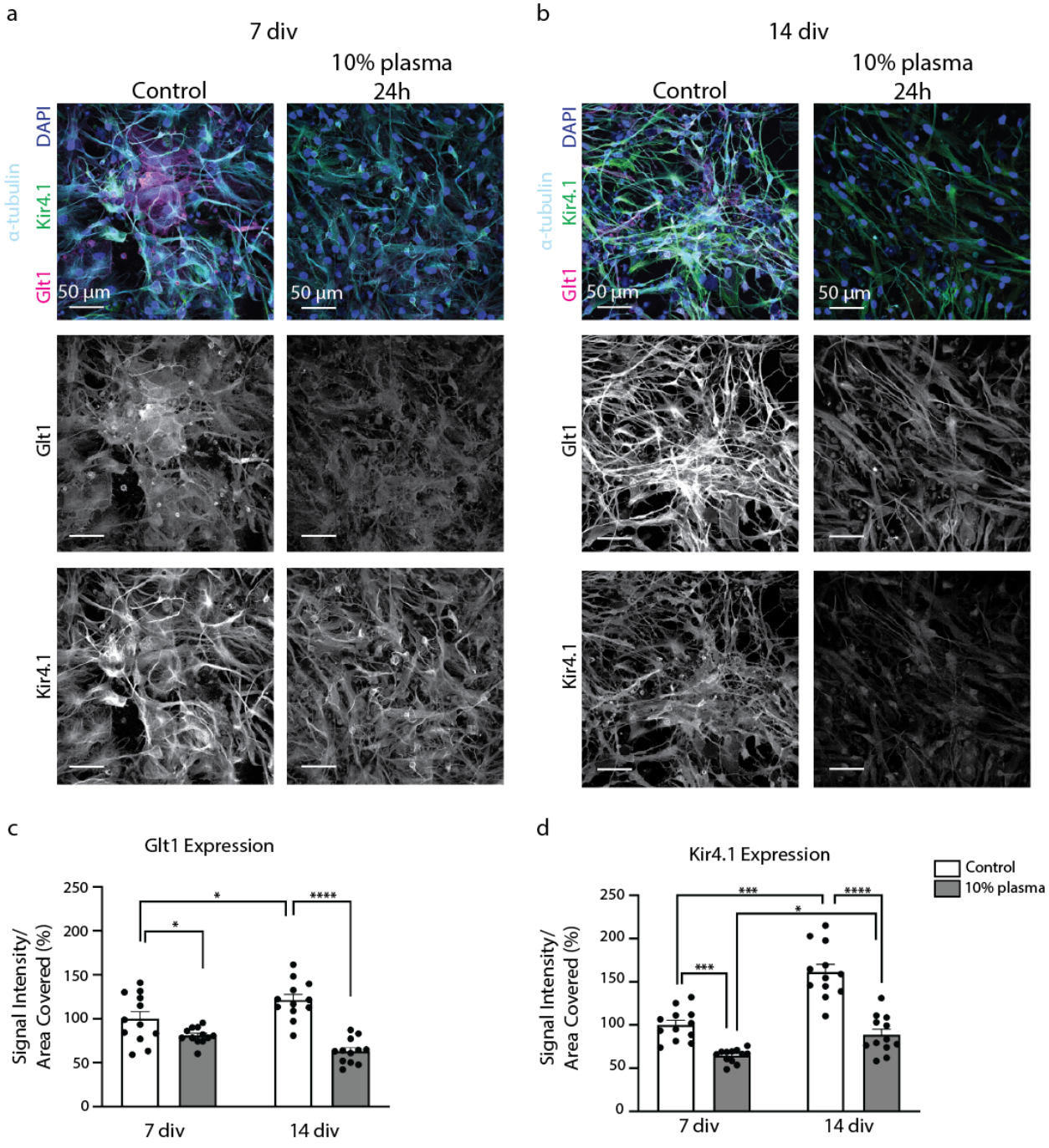

Figure 10: *Astrocytes maintained in media for different lengths of time experience loss of Glt1/Kir4.1 signal intensity after plasma exposure.* ***a.*** *Primary astrocytes maintained in serum-free media for 7 div demonstrated a similar atypical astrocyte phenotype after 24 h*

plasma exposure. ***b.*** *Control 14 div primary astrocytes showed increased Glt1/Kir4.1 signal intensity compared to control 7 div primary astrocytes and showed reduced Glt1/Kir4.1 signal intensity after plasma exposure.* ***c,d.*** *Glt1 and Kir4.1 expression was quantified by dividing the mean grayscale value by the area coverage of each protein, then data were normalized with respect to the control group. Data points represent ROIs. One independent culture was used for these experiments. (Glt1. Control 7 div, 100.00 ± 8.01, n=12. Plasma 7 div, 80.70 ± 2.68, n=12. Control 14 div, 121.27 ± 6.37, n=12, Plasma 14 div plate, 82.90 ± 11.03. Two-way ANOVA significant for treatment. p=0.0013. Sidak's multiple comparison tests. Control 7 div vs. Plasma 7 div, p=0.0400. Control 14 div vs. Plasma 14 div. p<0.0001. Two-way ANOVA significant for time in culture. p=0.0013. Sidak's multiple comparison tests. Control 7 div vs. Control 14 div, p= 0.0219. Plasma 7 div vs. Plasma 14 div. p=0.0163. Kir4.1. Control 7 div, 100.00 ± 5.28, n=12. Plasma 7 div, 64.51 ± 2.24, n=12. Control 14 div, 161.32 ± 8.94, n=12, Plasma 14 div, 88.70 ± 6.31. Two-way ANOVA significant for treatment. P<0.0001. Sidak's multiple comparison tests. Control 7 div vs. Plasma 7 div. p=0.0004. Control 14 div vs. Plasma 14 div. p<0.0001. Two-way ANOVA significant for time in culture. P<0.0001. Sidak's multiple comparison tests. Control 7 div vs. Control 14 div. p<0.0001. Plasma 7 div vs. Plasma 14 div. p=0.0613).*

3.6 Exposure to plasma in primary astrocyte cell culture mimics the atypical astrocyte response *in vitro*

To begin screening for individual factors that may trigger the atypical astrocyte phenotype, I heat-denatured fresh mouse plasma at 75 °C for 5 minutes to determine if a blood-borne protein induces loss of key homeostatic proteins in primary astrocytes. Then, I diluted the heat-denatured plasma in 5x B27 serum-free media before treating primary astrocytes with it and compared it to fresh plasma treatment and the controls. I found that treating primary astrocytes with heat-denatured plasma rescued Kir4.1, but not Glt1 expression, compared to the controls, suggesting that blood-borne proteins and other factors may drive the atypical astrocyte

response *in vitro* **(Fig. 11a-c)**.

In previous studies, fibrinogen leakage has been implicated in increased GFAP upregulation and glial boundary formation after focal TBI (Schachtrup et al., 2010) making fibrinogen one possible candidate to treat in primary astrocytes. First, I diluted fibrinogen to 400 mg/dL to reflect the concentration found in the bloodstream (Pedrazzani et al., 2016) in 5x B27 serum-free media, then added it to primary astrocytes for 24 hours. By comparing the Glt1/Kir4.1 expression in the fibrinogen treatments to the control and plasma groups, I found that Glt1 but not Kir4.1 expression was reduced **(Fig. 12a-c)**. Therefore, fibrinogen, in addition to other blood-borne factors, contributes to the atypical astrocyte phenotype *in vitro*.

While fibrinogen causes loss of some astrocytic homeostatic proteins *in vitro*, fibrinogen leakage rarely occurred after mTBI, allowing us to test another blood-borne factor that may trigger the development of the atypical astrocyte response. In previous studies, albumin leakage has been shown to cause epileptogenesis after TBI, so I investigated albumin's role in astrocytic protein expression *in vitro*. First, I diluted albumin to 4.5 g/dL in 5x B27 serum-free media before treating it on primary astrocyte cultures for 24 hours. Albumin treatment triggers the loss of Glt1, but not Kir4.1 signal intensity **(Fig. 13a-c)**.

Next, I investigated what downstream signaling pathways are activated by albumin and fibrinogen to trigger atypical astrocytes. Previous studies have demonstrated that albumin and fibrinogen activate the transforming-growth factor β (TGF- β) signaling pathway. (Ralay Ranaivo & Wainwright, 2010; Schachtrup et al., 2010; Senatorov et al., 2019). After these factors bind to the TGF- β receptor, it leads to the phosphorylation of SMAD protein complexes. Then, the SMAD complexes enter the nucleus and bind to the promoters to trigger the expression of different target genes. Here, I assess the activation of the TGF- β signaling pathway by measuring phosphorylated SMAD2 signal intensity in areas containing Glt1 loss. Increased phosphorylated SMAD2 signal intensity is observed at 6 hpi compared to the shams **(Fig. 14a,b)**. Overall, these data suggest that both albumin and fibrinogen exposure affect Glt1

expression via activation of the TGF- β signaling pathway, and that other factors may initiate Kir4.1 loss in primary cell cultures.

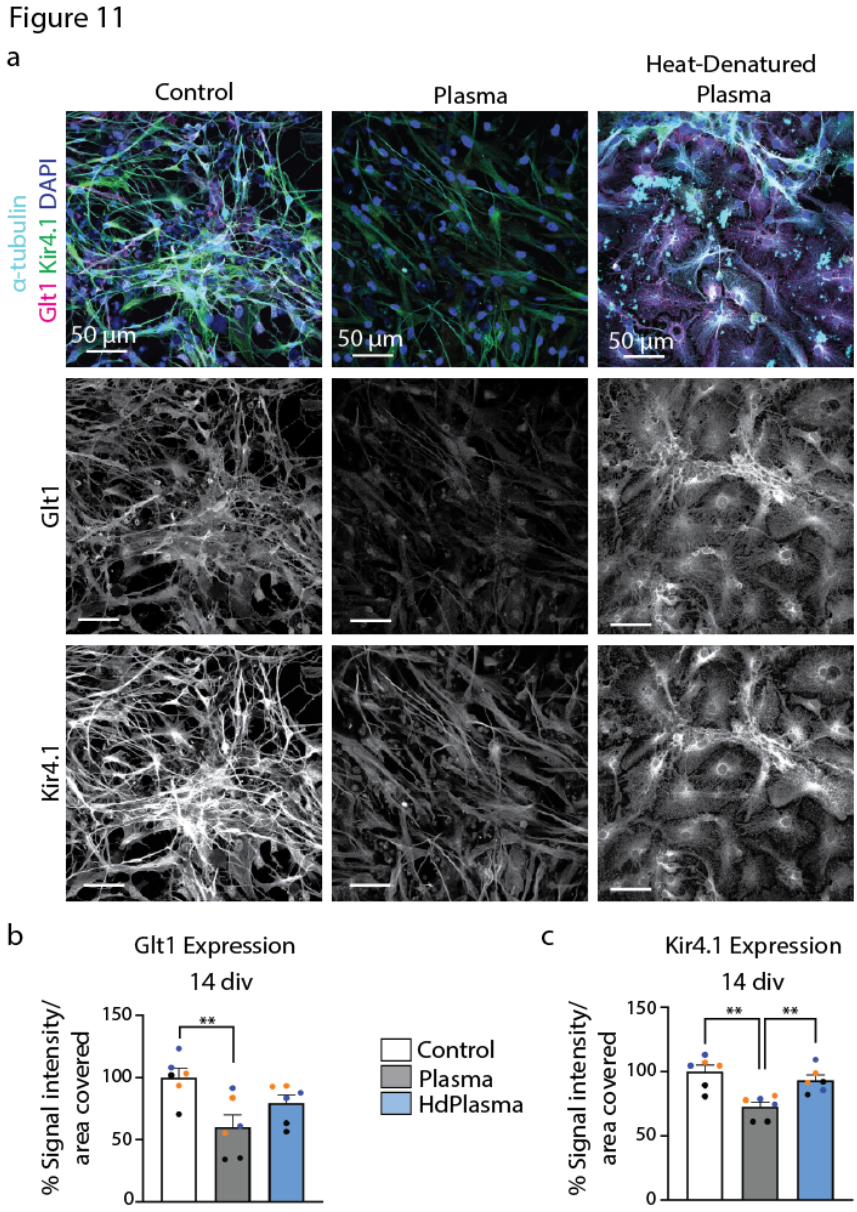

Figure 11: *Glt1 and Kir4.1 expression in astrocytes is reduced 24 hours after plasma treatment in vitro and is triggered by a plasma protein(s).* ***a.*** *Treatment with heat-denatured plasma rescued both Glt1 and Kir4.1 signal intensity in primary astrocyte cultures maintained in serum-free media for 14 div.* ***b,c.*** *Glt1 and Kir4.1 signal intensity was quantified by dividing the mean grayscale value by the area coverage of each protein, then data were normalized*

with respect to the control group. Data points represent coverslips and are color-coded with respect to each independent culture. Three independent cultures were used for these experiments. (Glt1. Control, 100 ± 7.133, n= 6 coverslips in 3 independent cultures; Plasma, 60.19 ± 9.743, n= 6 coverslips in 3 independent cultures; HdPlasma, 79.53 ± 6.402, n= 6 coverslips in 3 independent cultures. One-way ANOVA significant for treatment. p= 0.01. Tukey's multiple comparisons test. p<0.0001. Control vs. Plasma, p=0.0074; Control vs. HdPlasma, p0.1922; Plasma vs. HdPlasma, p=0.2257. Kir4.1. Control, 100 ± 5.006, n= 6 coverslips in 3 independent cultures; Plasma, 72.45 ± 3.705, n= 6 coverslips in 3 independent cultures; HdPlasma, 93.30 ± 4.001, n= 6 coverslips in 3 independent cultures. One-way ANOVA significant for treatment. p0.001. Tukey's multiple comparisons test. p<0.0001. Control vs. Plasma, p=0.001). Control vs. HdPlasma, p=0.0.5236. Plasma vs. HdPlasma, p0.0094). div= days in vitro, HdPlasma= Heat denatured plasma

Figure 12

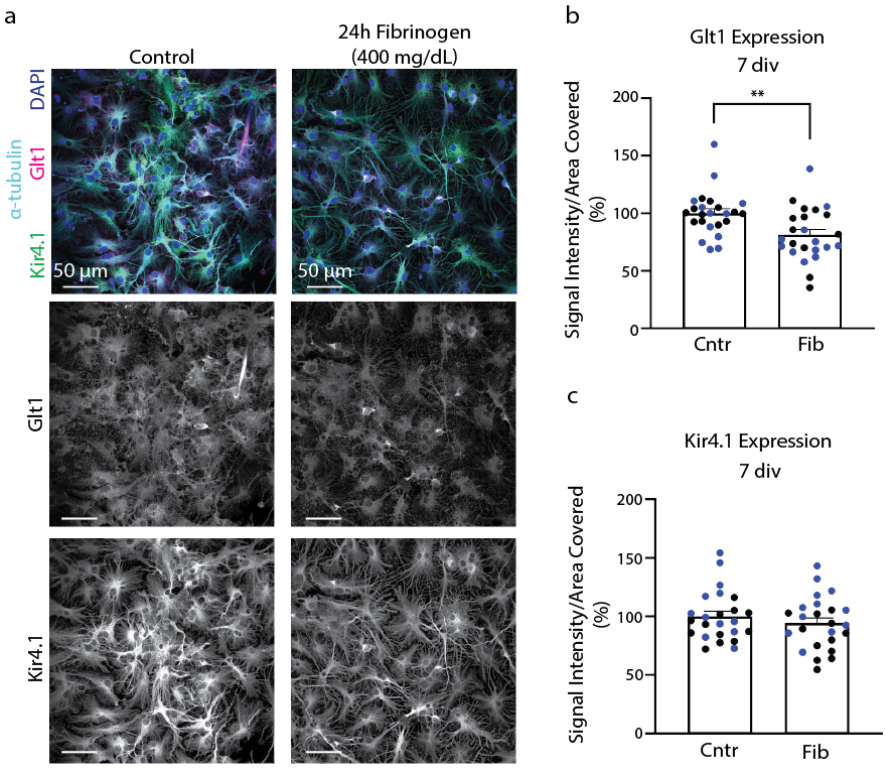

Figure 12: *Fibrinogen triggers Glt1, but not Kir4.1 loss in vitro.* ***a.*** *Fibrinogen triggered the*

loss of Glt1 signal intensity in astrocytes maintained in serum-free media for 7 div, while fibrinogen does not affect Kir4.1 signal intensity. ***b.,c.*** *Glt1 and Kir4.1 signal intensity was quantified by dividing the mean grayscale value by the area coverage of each protein, then data were normalized with respect to the control group. Data points represent ROIs. Two independent cultures were used in these experiments. (Glt1. Control, 100 ± 3.94, n= 24 ROIs in 2 independent cultures; Fibrinogen, 81.35 ± 4.648, n= 24 ROIs in 2 independent cultures; Unpaired t-test significant for treatment. p= 0.0037. Kir4.1. Control, 100 ± 4.359, n= 24 ROIs in 2 independent cultures; Plasma, 94.17 ± 4.57, n= 24 ROIs in 2 independent cultures. Unpaired t-test not significant for treatment. p=0.3609).*

Figure 13

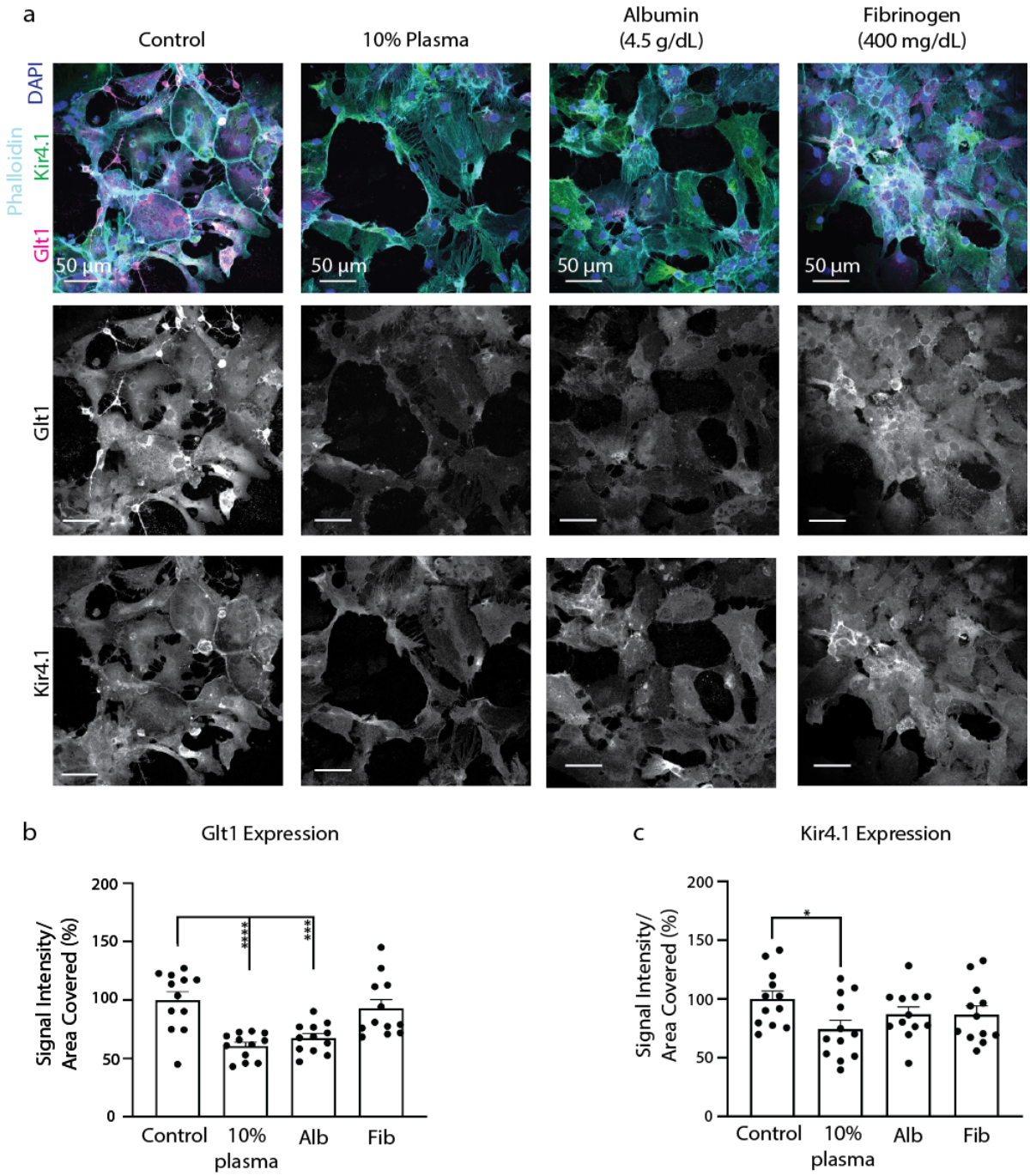

Figure 13: *Albumin triggers Glt1, but not Kir4.1 loss in vitro.* ***a.*** *Albumin triggered the loss of Glt1 signal intensity in astrocytes maintained in serum-free media for 14 div, while fibrinogen does not affect either Glt1 or Kir4.1 signal intensity.* ***b.,c.*** *Glt1 and Kir4.1 signal intensity was quantified by dividing the mean grayscale value by the area coverage of each protein, then*

data were normalized with respect to the control group. Data points represent ROIs. One independent culture was used for these experiments. (Glt1. Control, 100 ± 7.27, n= 12 ROIs in one independent culture; 10% plasma, 60.78± 3.21, n= 12 in one independent culture; Albumin, 67.62 ± 3.64, n=12 ROIs in 1 independent culture; Fibrinogen, 93.04 ± 7.31, n= 12 ROIs in one independent culture; One-way ANOVA significant for treatment. p< 0.0001. Tukey's multiple comparisons test. Control vs. Plasma, p<0.0001; Control vs. Albumin, p=0.0007; Control vs. Fibrinogen, p=0.7216. Kir4.1. Control, 100 ± 6.855, n= 12 ROIs in one independent culture; Plasma, 74.43 ± 7.54, n= 12 in one independent culture; Albumin, 87.32 ± 6.101, n=12 ROIs in one independent culture; Fibrinogen, 86.94 ± 7.290, n= 12 ROIs in one independent culture; One-way ANOVA not significant for treatment. p=0.0963. Tukey's multiple comparisons test. p=0.0963 Control vs. Plasma, p=0.0341; Control vs. Albumin, p=0.4382; Control vs. Fibrinogen, p=0.4141).

Figure 14

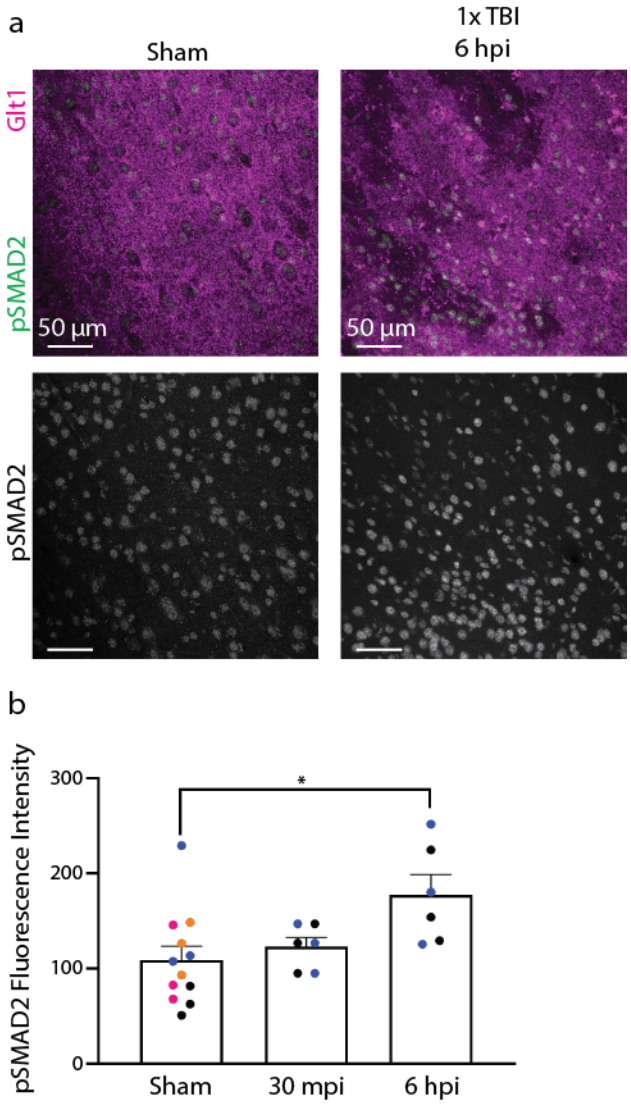

Figure 14: *mTBI triggers increased TGF- β signaling in atypical astrocytes.* ***a.*** *Increased pSMAD2 activation occurs in areas of atypical astrocytes at 6 hpi.* ***b.*** *Fluorescence intensity for pSMAD2 in areas of atypical astrocytes was calculated and reported as grayscale values. Data points are plotted by ROI and are color-coded for each animal. n=3 in sham group and n=2 in both 30 mpi and 6 hpi timepoints. (Sham, 109.2 ± 14.21, n=12; 1x TBI 30mpi, 123.0 ± 9.604, n=6, 1x TBI 6hpi, 177.8 ± 21.08. One-way ANOVA significant for post-injury timepoint, p=0.0204. Tukey's multiple comparisons test. Sham vs. 1xTBI 30mpi, p=0.8137; Sham vs. 1xTBI 6hpi, p=0.0164; 1xTBI 30mpi vs. 1xTBI 6hpi, p=0.1137).*

3.7 BBB leakage is not repaired after mTBI

3.7.1 BBB leakage is sustained at 64 days after mTBI

In previous studies that focused on focal TBI, BBB leakage and the presence of glial boundaries around the site of primary injury was found to last for several days after focal TBI. However, no glial boundaries are present after mTBI, yet the atypical astrocyte response persists for several months after injury. Thus, we wanted to determine whether BBB repair occurs in areas of atypical astrocytes after mTBI.

At 7 dpi, 14 dpi, and 64 dpi, mice were given retro-orbital injections of Cadaverine 30 minutes before perfusion to assess whether BBB leakage is contained after mTBI. We have shown that BBB leakage was observed at all three timepoints **(Fig. 15a-c)**. Next, we examined BBB leakage after single and repeated mTBI at 1 dpi and 7 dpi. In addition to showing that both single and repeated mTBI caused significant Cadaverine leakage compared to the shams, Cadaverine leakage was doubled in mice subjected to repeated mTBI at 7 dpi (**Fig. 15d)**. Here, we demonstrated that there is a lack of BBB repair, resulting in increased BBB leakage that overlap with atypical astrocytes in the long-term after mTBI. Also, we found that repeated mTBIs trigger more BBB leakage, potentially leading to more secondary brain injury.

3.7.2 BBB properties remain disrupted at 64 days after mTBI

To identify the BBB properties that lead to prolonged BBB damage after mTBI, we measure ZO-1 vessel coverage and signal intensity after 64 dpi. While ZO-1 signal intensity is slightly reduced, ZO-1 vessel coverage is reduced significantly at 64 dpi **(Fig 15e-g)**, suggesting that prolonged BBB damage is due to the loss of proteins that maintain tight junction function.

Next, we want to determine if increased BBB damage caused entry of peripheral immune cells into the brain parenchyma after mTBI; we perform IHC against CD45, which labels lymphohematopoietic cells (Frik et al., 2018) such as monocytes. Typically, immune cells are present in the meninges in the shams, but I observed an average of about 5-10 cells in the cortex at 1 dpi and 7 dpi (**Fig. 15h,i**). However, number of CD45+ cells returned to similar values

found in the shams at 64 dpi, suggesting that BBB damage after mTBI does not induce massive immune cell infiltration compared to more severe TBI.

Figure 15

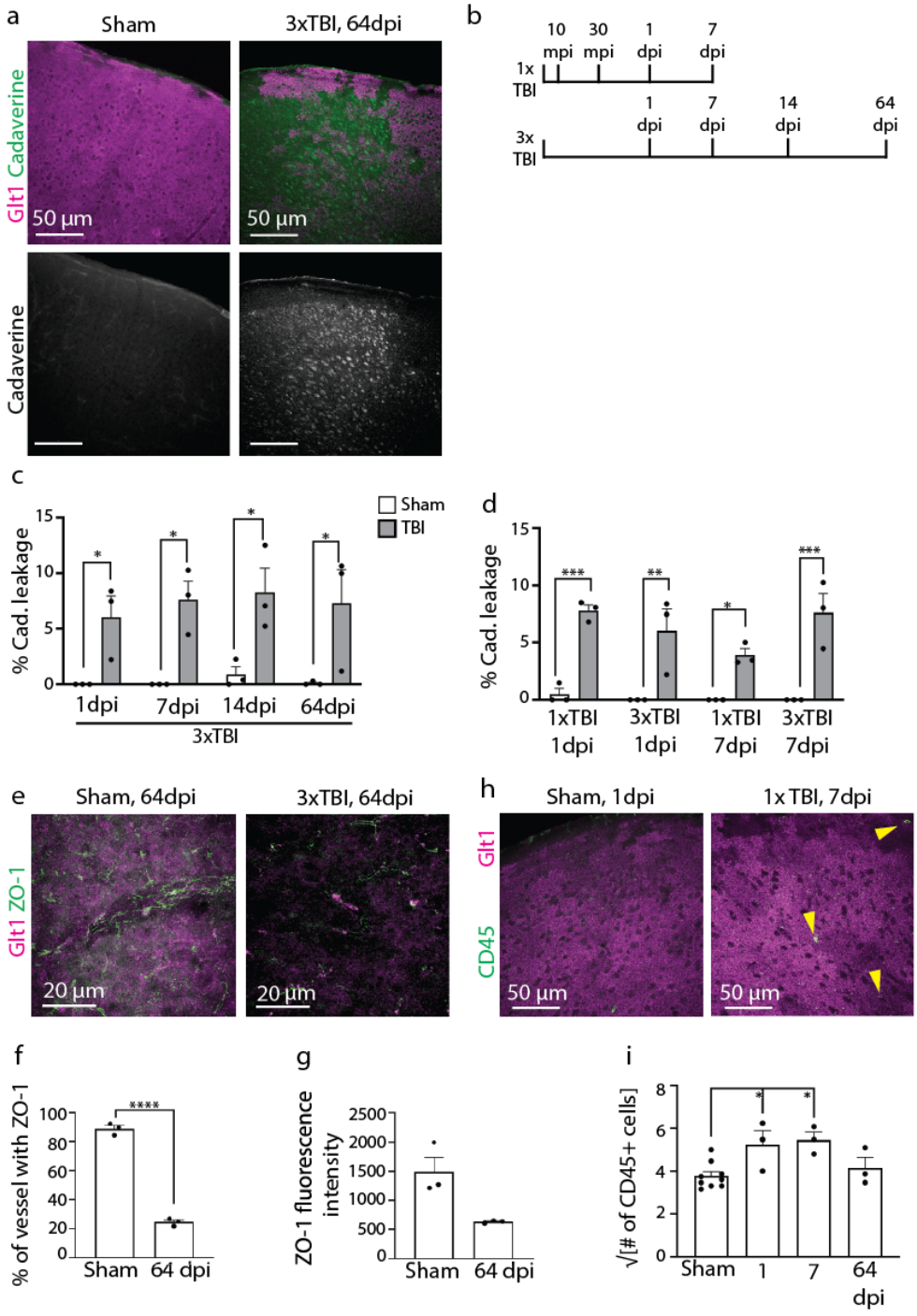

Figure 15: *The BBB is not repaired after mTBI.* ***a.*** *Cadaverine leakage was still present at 64 dpi.* ***b.*** *Mice were examined at later timepoints after 3xTBI and 1xTBI.* ***c.*** *Cadaverine leakage*

was quantified at later timepoints after 3xTBI as the percent area of total cortex and plotted by animal. (3x Sham 1dpi, 0 ± 0, n= 3; 3xTBI 1dpi, 6.0253 ± 1.9186, n= 3; 3x Sham 7dpi, 0 ± 0; 3xTBI 7dpi, 7.5890 ± 1.6852, n= 3; 3x Sham, 0.8845 ± 0.6973; 3xTBI 14dpi, 8.2640 ± 2.1837, n= 3; 3x Sham 64dpi, 0.0963 ± 0.0963; 3xTBI 64dpi, 7.2668 ± 3.051, n= 3. Kruskal-Wallis test significant for post-injury timepoint, p< 0.0001. Sidaks's multiple comparisons test. 3xSham vs. 3xTBI 1dpi, p= 0.0717; Sham vs. 3xTBI 7dpi, p=0.0178; Sham vs. 3xTBI 14dpi, p= 0.0215; Sham vs. 3xTBI 64dpi, p=0.0260). ***d.*** *Cadaverine leakage quantifications were compared between the 1dpi and 7dpi timepoints after either 1xTBI or 3xTBI. (1x Sham 1dpi, 0.0493 ± 0.0493, n=3; 1xTBI 1dpi, 7.7900 ± 0.50.62, n= 3; 1x Sham 7dpi, 0 ± 0, n=3; 1xTBI 7dpi, 6.0253 ± 1.9186, n= 3; 3x Sham 1dpi, 0 ± =,n=3; 3xTBI 1dpi, 3.9183 ± 0.5503, n= 3; 3x Sham 7dpi, 0 ± 0,n=3; 3xTBI 7dpi, 3xTBI 7dpi, 7.5890 ± 1.6853, n=3. Two-way ANOVA significant for number of injuries, p<0.0001; 1xSham 7dpi vs. 1xTBI 7dpi, p=0.0415;. 3xSham 7dpi vs. 3xTBI 7dpi, p= 0.0002; 1xSham 1dpi vs. 1xTBI 1dpi, p=0.0002, 3xSham vs 3xTBI 1dpi, p= 0.0.0002; Tukey's multiple comparisons test. 1xSham 1dpi vs 3xSham 1dpi. p=0.9898; 1xSham 1dpi vs. 1xSham 7dpi, p=0.9829; 1xSham 1dpi vs. 3xSham 7dpi, p=0.9829; 3xSham 1dpi vs. 1xSham 7dpi, p>0.9999; 3xSham 1dpi vs. 3x Sham 7dpi, p>0.9999; 1xSham 7dpi vs. 3xSham 7dpi, p>0.9999; 1xTBI 1dpi vs. 1xTBI 7dpi, p= 0.0.05; 3xTBI 1dpi vs. 3xTBI 7dpi, p= 0.5737* ***e.*** *Lack of ZO-1 persists at 64 dpi.* ***f.*** *The continuity of ZO-1 labeling along vessels was quantified at 64dpi in areas of atypical astrocytes as shown in* ***Fig 5b.*** *(Sham, 11.02 ± 2.602, n= 3; 3xTBI 8 wpi, 75.08 ± 1.531, n= 3. Unpaired t test for Sham vs. 3xTBI 8 wpi, p< 0.0001).* ***g.*** *Fluorescence intensity for the ZO-1 lines drawn in* ***e*** *and were reported as grayscale values. (Sham, 1492 ± 251.5, n= 3; 3xTBI 8 wpi, 632.5 ± 14.13, n= 3; Unpaired t test for Sham vs. 3xTBI 8 wpi, p= 0.0755).* ***h.*** *Clusters of CD45$^+$ cells (indicated by yellow arrowheads) appeared in the cortex after mTBI, while in sham mice, these clusters were found localized to the meninges.* ***i.*** *Immune cell infiltration was quantified by taking the square root of the total number of CD45$^+$ cells per animal. (Sham, 3.772 ± 0.2013, n = 9; 1dpi, 5.241 ± 0.0.6588, n= 3; 7 dpi, 5.452 ±*

0.3717, n= 3; 64 dpi, 4.145 ± 0.4912, n= 3. One-way ANOVA significant for post-injury timepoint. p< 0.0001 Tukey's multiple comparisons tests. p=0.0106. Sham vs. 1 dpi, p=0.0461; Sham vs. 7 dpi, p=0.0209, Sham vs. 64 dpi, p=0.8754; 1 dpi vs. 7 dpi, p=0.851 1 dpi vs. 64 dpi, p=0.1032; 7 dpi vs. 64 dpi, p=0.1872).

3.8 Loss of astrocytic factors that maintain BBB integrity occurs after mTBI

In addition to removing excess neurotransmitters and ions from the extracellular space, astrocytes maintain BBB integrity by interacting directly with ECs via astrocytic endfeet. Thus, we hypothesized that prolonged BBB leakage after mTBI is caused by the loss of astrocyte-secreted proteins that maintain the BBB and stabilize endfeet to the blood vessels. Astrocyte endfeet function within the neurovascular unit depends on the dystrophin-associated glycoprotein complex (DAGC), a transmembrane scaffolding machine that anchors astrocyte endfeet to the basement membrane. One protein from the DAGC that was examined via IHC is β -Dystroglycan (bDG), which outlines the endfeet in the sham brain slices. After mTBI, bDG was reduced after 1 dpi **(Fig. 16a, b)**.

The DAGC interacts with the basement membrane, which is comprised of proteins, such as laminin and collagen IV that anchor neighboring cells (Hoddevik et al., 2020) Similarly, collagen IV and laminin expression were lost after mTBI, as well **(Fig. 17a, b)**. Collagen IV and laminin are substrates of matrix metalloproteinase-9 (MMP9), which is a proteinase that breaks down the extracellular matrix of neighboring tissue. In the context of brain pathology, MMP9 expression has been shown to be upregulated in astrocytes (Mhatre et al., 2004). Using IHC, we found that MMP9 expression appears to be limited to neurons, and its intensity was unaffected in atypical astrocytes after mTBI **(Fig. 18a,b)**. Overall, these data suggest that mTBI triggers reduced bDG and basement membrane protein expression and may contribute to sustained BBB damage.

Aquaporin-4 (AQP4) is responsible for transporting water between the brain parenchyma and the periphery. While AQP4 contributes to maintaining the BBB's metabolic

barrier, its function depends on the function of the DAGC. As expected, we observed a reduction in AQP4 labeling along blood vessels in atypical astrocyte areas at 1 dpi (**Fig. 16c, d)**. However, Tdtomato+ astrocyte endfeet remained intact but contained little AQP4 expression after mTBI. Therefore, these data highlight that astrocyte endfeet protein expression, but not the endfeet themselves, are disrupted after mTBI.

While sonic hedgehog (Shh) signaling is involved in the formation of the nervous system during development, it has been shown to be upregulated in reactive astrocytes after TBI and is implicated in BBB maintenance (Allahyari, Clark, Shepard, & Garcia, 2019; Alvarez et al., 2011). Thus, we used IHC against the Shh antibody in reporter mice expressing Tdtomato+ astrocytes and subjected to mTBI. In the sham tissues, we found that Shh was expressed in the astrocytic processes. However, this Shh expression at the processes was lost after 3 dpi. Interestingly, Shh expression appears to be upregulated in ECs after mTBI, yet it is not sufficient to halt BBB leakage after injury **(Fig. 16e)**.

Figure 16

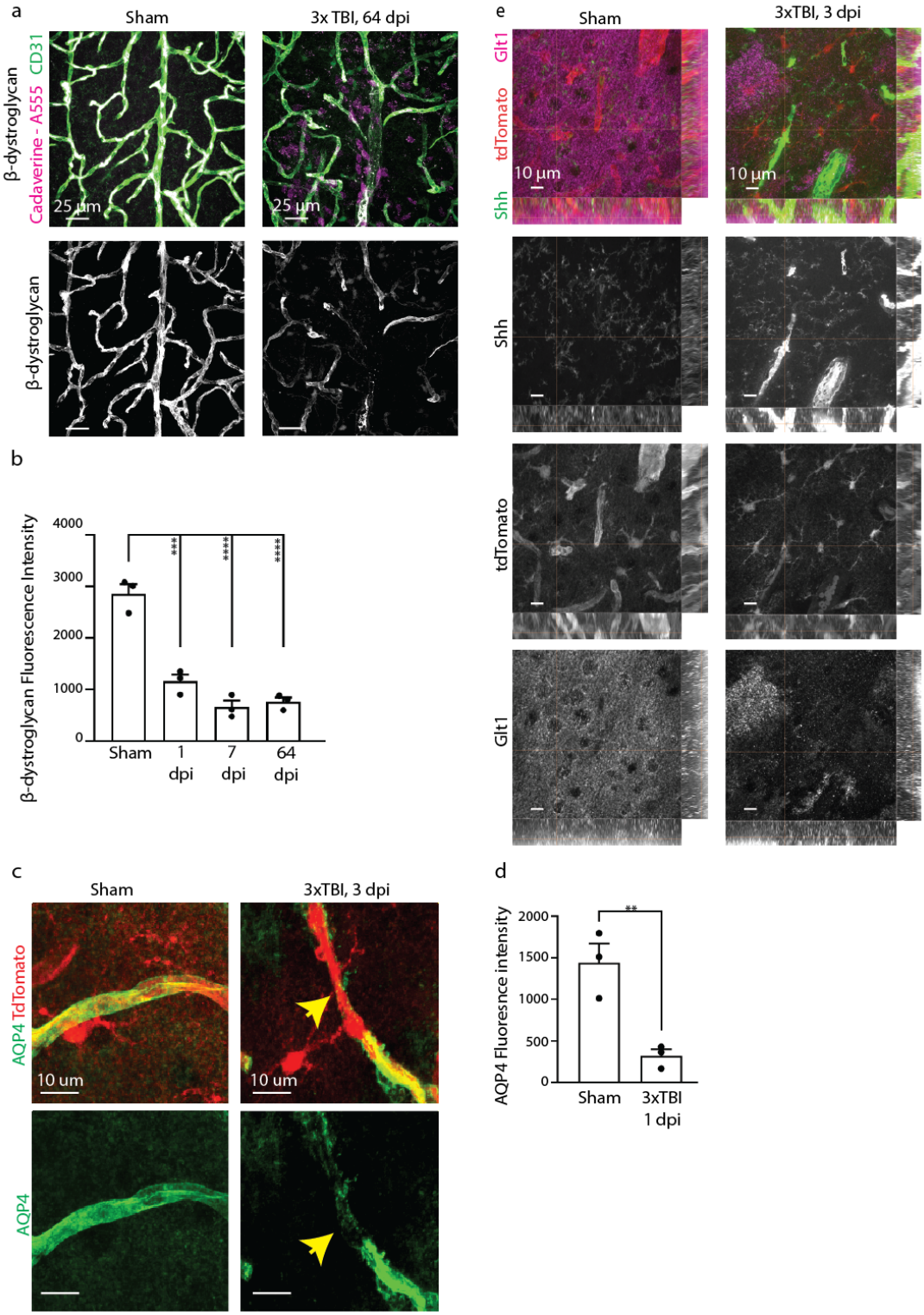

Figure 16: *BBB leakage induces loss of astrocytic-secreted proteins responsible for BBB maintenance after mTBI.* ***a.*** *β-dystroglycan is significantly lost after mTBI at 1 dpi.* ***b.***

Fluorescence intensity for the β-dystroglycan in areas of atypical astrocytes was calculated and reported as grayscale values. Data points are plotted by animal. (Sham, 2856 ± 188.7, n=3; 3xTBI 1 dpi, 1158 ± 135, n=3, 3xTBI 7 dpi, 659.9 ± 123.5, n=3; 3xTBI 64 dpi, 760.2 ± 83.51. One-way ANOVA significant for post-injury timepoint. p<0.0001. Tukey's multiple comparisons test. Sham vs. 1 dpi, p=0.0001; Sham vs. 7 dpi, p<0.0001; Sham vs. 64dpi, p<0.0001; 1 dpi vs. 7 dpi, p=0.1244; 1 dpi vs. 64 dpi, p=0.2503; 7 dpi vs. 64 dpi, p=0.9533). ***c.*** *Astrocytic endfeet remain intact, but aquaporin-4 (AQP4) is reduced after mTBI.* ***d.*** *Fluorescence intensity of AQP4 in areas of atypical astrocytes was calculated and reported as grayscale values. Data points are plotted by animal. (Sham, 1440 ± 229.7, n=3, 3xTBI 1dpi, 320.6 ± 78.54, n=3. Unpaired t test for Sham vs. 3xTBI. p=0.0099).* ***e.*** *Sonic hedgehog (Shh) signaling is localized mostly along blood vessels after mTBI, whereas in the shams, Shh signaling is located more along the fine processes of tdTomato+ astrocytes.*

Figure 17

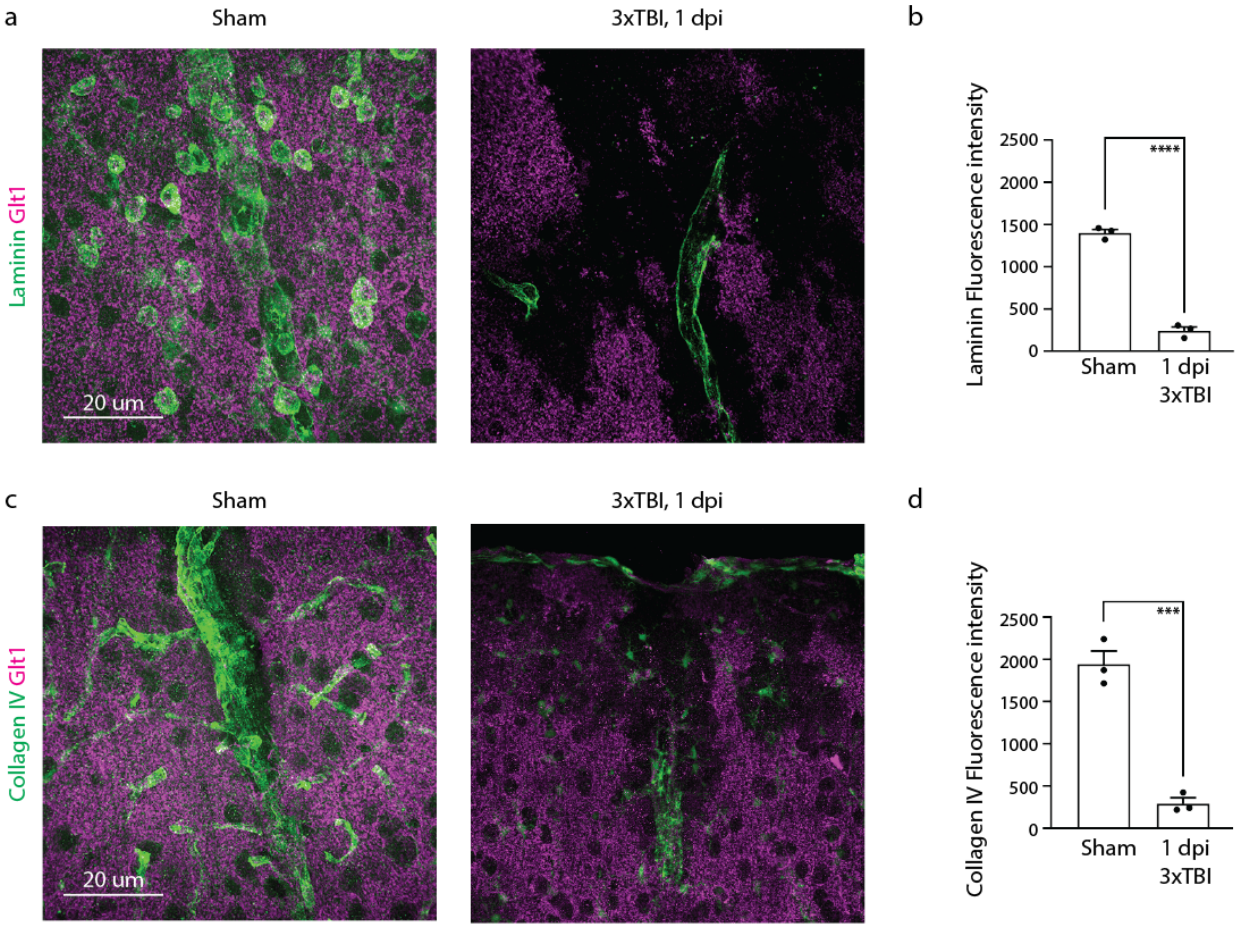

Figure 17: *Basement membrane proteins are lost after mTBI.* ***a.*** *Laminin is reduced in atypical astrocytes at 1 dpi.* ***b.*** *Fluorescence intensity of laminin in areas of atypical astrocytes was calculated and reported as grayscale values. Data points are plotted by animal. (Sham, 1402 ± 41.16, n=3, 3xTBI 1dpi, 243.1 ± 44.40, n=3. Unpaired t test for Sham vs. 3xTBI, p<0.0001.* ***c.*** *Collagen IV is lost in atypical astrocytes after mTBI.* ***d.*** *Fluorescence intensity for collagen IV in areas of atypical astrocytes was calculated and reported as grayscale values. Data points are plotted by animal. (Sham, 1943 ± 155.7, n=3, 3xTBI 1dpi, 293.4 ± 65.36. Unpaired t test for Sham vs. 3xTBI, p=0.0006).*

Figure 18

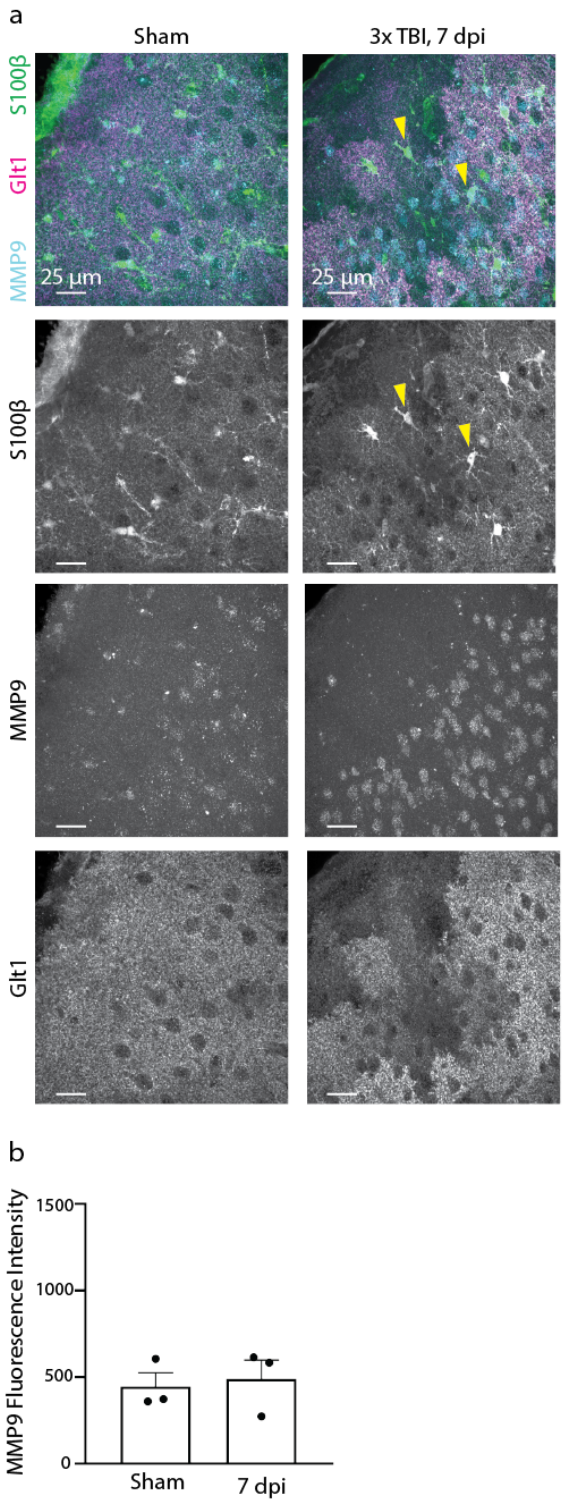

Figure 18: *mTBI does not cause changes in MMP9 expression.* ***a.*** *Matrix-metalloproteinase-9 (MMP-9) remains unaffected in atypical astrocytes after mTBI.* ***b.*** *Fluorescence intensity for*

MMP-9 in areas of atypical astrocytes was calculated and reported as grayscale values. (Sham, 446.1 ± 80.03, n=3; 3xTBI 7dpi, 490.1 ± 108.6, n=3. Unpaired t test for Sham vs. 3xTBI, p=0.7622).

4 Discussion

4.1 mTBI is sufficient to trigger BBB damage

First, our data show that a single mTBI is sufficient to cause BBB leakage, and this leakage overlaps with areas containing atypical astrocytes as early as 10 mpi. In our studies, we measure the amount of BBB leakage in the cortex, but we did not determine if this leakage was observed in other brain regions. In clinical studies that use DCE-MRI, increased BBB permeability was found in the hippocampus, as well as in other gray and white matter regions, of older patients who experienced early-onset Alzheimer's Disease (Nation et al., 2019; van de Haar et al., 2016). While patient data suggest that neurodegenerative disease results in increased BBB permeability in multiple brain regions, one possible interpretation of our data could be that BBB damage occurs predominately in the cortex after mTBI. However, more studies that include determining in what other brain regions BBB leakage is found as well as how much leakage is taking place in these areas after mTBI need to be conducted.

One of the major drawbacks of the standard imaging techniques used to assess BBB damage in patients is the lack of sensitivity in detecting immediate changes in BBB permeability (Cash & Theus, 2020). In our studies, we used a small tracer dye, such as Cadaverine, to identify subtle signs of BBB disruption. However, Cadaverine leakage does not provide insight into what factors are leaking into the brain parenchyma after injury. In both human and rodent studies, tracer dyes, such as Evans blue, bind to as albumin and are used to assess for BBB permeability (Y. Xu et al., 2019; Yao, Xue, Yu, Ni, & Chen, 2018). To begin elucidating the causal link between BBB leakage and the development of long-term neurological consequences, labeling blood-borne factors that differ in molecular weight can help to identify possible cellular mechanisms that are activated by these factors after injury.

4.2 Does the primary astrocyte culture model mimic what is observed after mTBI?

In previous cell culture studies, astrocytes have been maintained in media containing FBS.

To determine how astrocytes respond to blood-borne factors and if this response mimics what is observed *in vivo*, we used a chemically defined cell culture system where astrocytes are cultured in the absence of serum-based factors found in FBS. In our endothelial ablation model, I observe Glt1 and Kir4.1 loss occurring after 6 hpa and 1 dpa respectively. While I observe reduction in both Glt1 and Kir4.1 signal intensity after 24 hours of plasma exposure *in vitro*, I did not examine at what timepoint after plasma exposure does reduction in both proteins occur. Thus, the next step would be to determine if reduction of either Glt1 or Kir4.1 at several timepoints between 2 and 24 hours after plasma exposure. In addition to identifying when both Glt1 and Kir4.1 expression are reduced after plasma exposure, we should investigate if plasma exposure causes changes in expression of other astrocytic markers that were examined after mTBI to assess the validity of the primary astrocyte cell culture in mimicking the changes observed after injury.

One of the main challenges in characterizing brain pathology after mild TBI is the difficulty in determining whether worsening neurological consequences arise from mechanical strain or secondary injury (Fehily & Fitzgerald, 2017). To overcome this challenge, I culture astrocytes and treat them with plasma to determine how they respond to blood-borne factors independent of the responses from other cell types. Under healthy conditions, astrocytes maintain synapses by secreting thrombospondins and responding to neuronal activity (Allen & Eroglu, 2017). In response to mTBI, leakage of blood-borne factors triggers the loss of neuronal markers and post-synaptic punta (Muñoz-Ballester et al, 2022). However, it is unclear as to whether these changes in both astrocytes and neurons are happening in parallel or if crosstalk is occurring between both cells to trigger changes in their respective protein expressions in response to BBB damage. To address this question, we can develop a co-culture consisting of astrocytes and neurons to determine how astrocytic protein expression is affected by its interaction with neurons after exposure to plasma.

4.3 What plasma-borne factors trigger atypical astrocytes?

To begin screening for different blood-borne factors, we used heat-denaturation to determine if blood-borne proteins are involved in inducing an atypical astrocyte phenotype *in vitro*. After treating primary astrocytes with heat-denatured plasma, it rescued Kir4.1 but not Glt1 after 24 hours of treatment. Typically, plasma proteins begin denaturing at around 40-45^{o}C, and globulins denature at around 60 ^{o}C (Akazawa-Ogawa, Nagai, & Hagihara, 2018; Vazquez & Larson, 2013), so I denature plasma at 75 ^{o}C to ensure that all plasma-borne proteins would be inactivated before treatment. However, one of the drawbacks to using heat-denaturation is that heat also triggers oxidation of lipids (Reis et al., 2021), which can interact with astrocytes and affect their morphology, protein expression, and function as well. Therefore, we can use techniques, such as size-exclusion chromatography (Some, Amartely, Tsadok, & Lebendiker, 2019) to allow for a more sensitive screening process for different blood-borne factors.

One of the first plasma proteins we examined was fibrinogen, due to its role in triggering astrogliosis after TBI (Schachtrup et al., 2010). In our *in vitro* studies, we showed that fibrinogen exposure reduces Glt1 expression but not Kir4.1. However, due to the sparse number of fibrinogen deposits present after mTBI, the findings suggest that other plasma-borne factors cause the atypical astrocyte response after injury. Also, we have demonstrated that albumin exposure triggers a reduction in Glt1 *in vitro*. These data imply that the leakage of blood-borne factors induces atypical astrocytes by reducing Glt1 expression. Recently, we demonstrated that Glt1 loss occurs as early as 5 mpi (Muñoz-Ballester et al., 2022) and is sustained for months after injury (Shandra et al., 2019). Also, we observed Kir4.1 loss at 1 dpi, but we have not examined whether this loss occurs at earlier timepoints because areas of Kir4.1 loss are more difficult to identify than areas of Glt1 loss. These observations could be due to differences in how sensitive different astrocytic proteins are to exposure to blood-borne factors. However, more astrocytic proteins would need to be examined *in vitro* to determine how they respond to either

albumin or fibrinogen treatment.

While both fibrinogen and albumin cause loss of Glt1 signal intensity in primary astrocytes, it is worth noting that albumin triggered loss of Glt1 signal intensity after one independent culture, suggesting that albumin may drive the induction of atypical astrocytes compared to other blood-borne proteins. Also, it is important to determine if loss of Glt1 translates to reduced glutamate uptake. In primary astrocyte cultures, albumin exposure causes an increase in extracellular glutamate in addition to reduction in the mRNA expression for SLC1A2, the gene that encodes for Glt1 (David et al., 2009). After measuring whole-cell glutamatergic currents, changes in extracellular glutamate uptake and SLC1A2 expression led to increased excited post-synaptic potentials (EPSPs) in NMDA receptors. While it suggests that albumin causes increased excitability via loss of Glt1, determining how albumin affects other astrocytic proteins that play a role in homeostasis *in vitro* would help to determine how exposure to plasma-borne factors mimics what is observed after injury.

Protein	**Treatment Groups**				
	2 hour plasma	24 hour plasma	24 hour Denatured plasma	24 hour fibrinogen	24 hour albumin
Glt1	No change	Reduced in both 7 d*iv* and 14 d*iv* astrocytes	Reduced in 14 d*iv* astrocytes	Reduced in 7 d*iv* astrocytes after two cultures. No change in 14 d*iv* astrocytes	Reduced in 14 d*iv* astrocytes

				after one culture	
Kir4.1	No change	Reduced in both 7 d*iv* and 14 d*iv* astrocytes	No change	No change	No change

Table 3: *Summary of changes in astrocytic protein signal intensity observed in ICC after treatment.*

4.4 What downstream signaling pathways are activated after blood-borne factor leakage?

Previous studies that use focal TBI models revealed that both fibrinogen and albumin interact with the TGF- β signaling pathway and have been implicated in Alzheimer's disease and epileptogenesis via pharmacological inhibition or genetic knockout of the TGF- β receptor (Petersen, Ryu, & Akassoglou, 2018; Ralay Ranaivo et al., 2012; Senatorov et al., 2019). Activation of the TGF- β signaling pathway leads to phosphorylation of SMAD protein complexes that act as transcription factors, which are shuttled into the nucleus to trigger the transcription or repression of various target genes (Derynck & Budi, 2019).

In the context of astrocyte response, inhibition of SMAD2/3 reduces the formation of glial boundaries after ischemic stroke (Zhang et al., 2018). While activation of SMAD protein complexes that trigger the transcription of different target genes, phosphorylation of SMAD protein complexes that act as repressors has been implicated in the onset of neurodegenerative disease. For example, activating the TGF- β receptor also initiates production of SMAD

ubiquitin regulatory factors (SMURF), which has been linked to the development of neurodegenerative disease (Nakamura et al., 2013).

Previous studies have highlighted that thrombin causes the upregulation of MMP9 and other factors that break down the BBB via interaction with the protease-activated receptor (PAR) pathway (Lin et al., 2013). In the context of pathology, thrombin extravasation has been linked to depressive-like behavior in mice subjected to a closed-skull midline TBI. More specifically, inhibiting the PAR pathway via pharmacological targeting of Rho kinase (ROCK) rescued the reduction of Glt1 after TBI, (Piao, Holloway, Hong-Routson, & Wainwright, 2019). While it is important to identify possible downstream signaling pathways that lead to long-term neurological consequences after TBI, the next steps would be to conditionally knockout these different pathways specifically in astrocytes before inducing mTBI to determine if the astrocytic markers lost after injury are restored. These findings would thus help to identify the causal link between BBB leakage and the presence of atypical astrocytes after mTBI.

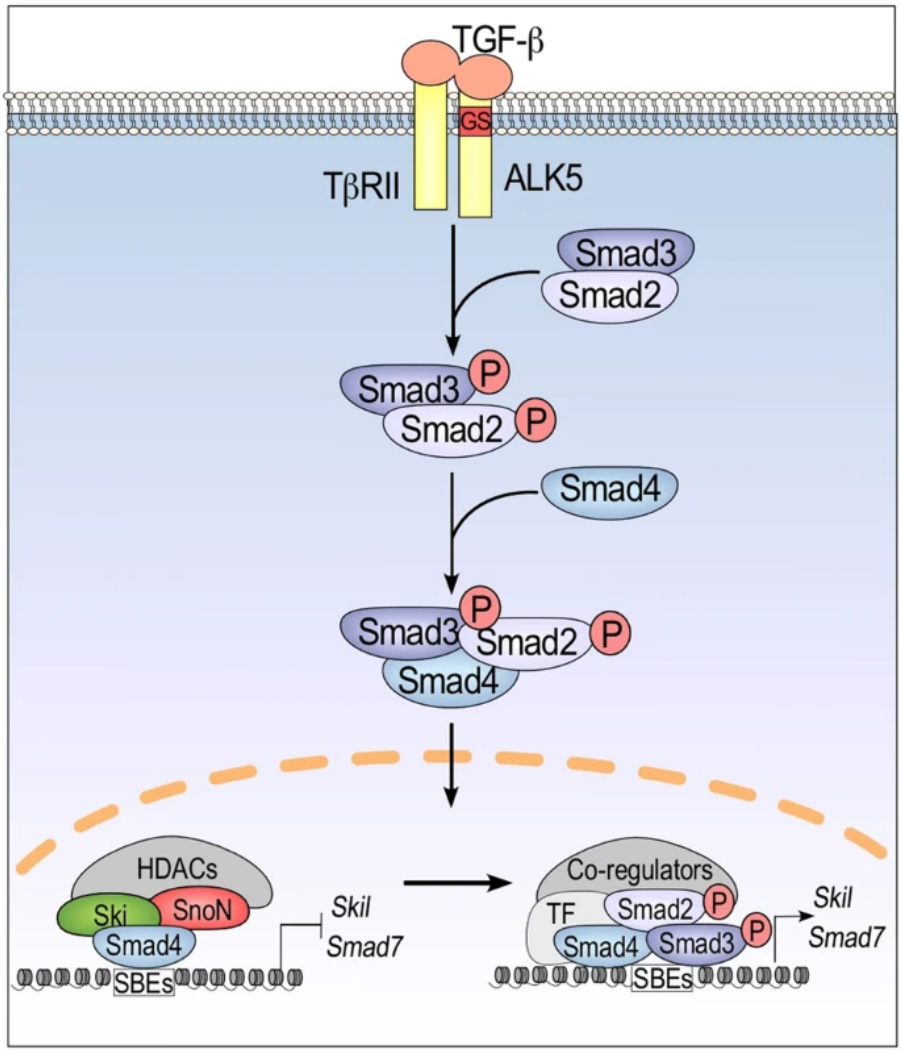

Figure 19: *Diagram of the TGF- β signaling pathway. After fibrinogen/albumin bind to the TGF- β receptor, it phosphorylates the protein domains, SMAD. SMAD proteins form a protein complex and it shuttled into the cell nucleus to trigger expression of target genes activated by the TGF- β signaling pathway. Source: (Tecalco-Cruz, Ríos-López, Vázquez-Victorio, Rosales-Alvarez, & Macías-Silva, 2018)*

4.5 How do astrocytes maintain BBB integrity after mTBI?

Astrocytes maintain BBB integrity through their physical contact with blood vessels via endfeet. After mTBI, the astrocyte endfeet remained attached to the blood vessels except for the loss of collagen IV and laminin, showing that part of the NVU is partially disrupted in response to injury. However, studies that use electron microscopy reveal degeneration of the astrocyte

endfeet following blast injury within several months after injury (A. T. Clark, Abrahamson, Harper, & Ikonomovic, 2022; Gama Sosa et al., 2019). One possible explanation for the connection between both the endfeet and blood vessel being mostly intact in our mTBI/ concussion studies is that astrocyte endfeet may detach from the ECs at a later timepoint than 1 dpi. Therefore, by examining the interaction between Tdtomato+ astrocyte endfeet and blood vessels after later timepoints, it can provide insight as to whether the endfeet detach from the blood vessels in response to mTBI.

In addition to astrocytes' direct contact with the BBB, astrocytes maintain the BBB's protective properties by secreting factors that maintain its integrity. In recent studies, upregulation of Shh signaling has been implicated in BBB maintenance (Allahyari et al., 2019; Xing et al., 2020). Here, we found that Shh signaling in astrocyte processes is reduced after mTBI. While these findings suggest that mTBI inhibits Shh signaling in astrocytes, it is difficult to determine how Shh signaling from astrocytes interacts with ECs to cause prolonged BBB leakage based on our mTBI data. One possible mechanism for BBB maintenance via Shh signaling is that some studies suggest that Shh signaling prevents EC apoptosis via activation of the protein, Patched-1 (PTCH1) (Michinaga & Koyama, 2019; Zhu et al., 2015). In future studies, we can investigate the role of PTCH1 in maintaining BBB integrity after mTBI.

After mTBI, we observe that bDG and AQP4 signal intensity are reduced, suggesting that loss of these astrocyte-secreted factors prolonged BBB leakage after injury. In a mouse model of Duchenne muscular dystrophy, bDG and AQP4 are reduced. However, both of those proteins and BBB integrity were rescued after these mice were treated with PDN (Annese et al., 2016; Tamma et al., 2013). After mTBI, basement membrane proteins, bDG, and AQP4 are reduced after 1 dpi, so it is difficult to determine loss of basement membrane proteins triggers loss of DAGC proteins or vice versa after BBB leakage. Thus, earlier timepoints need to be examined to determine when each of these proteins are reduced after injury to mitigate the progression of BBB leakage if these proteins are used as therapeutic targets.

4.6 The BBB fails to repair itself after mTBI

After focal TBI, BBB leakage lasts for about 10-14 days, implying that glial boundary formation around the site of primary damage is responsible for BBB repair. Also, tight junction function remained disrupted in areas of atypical astrocytes long-term, and it is unclear as to whether the BBB can repair itself after injury. Studies that examine whether tight junctions are restored have been mostly performed *in vitro* and in non-neural tissue (Chen et al., 2018). Therefore, we investigated how astrocytes maintain the BBB *in vivo* by using a genetic ablation mouse model that targets a small subset of astrocytes. In one of our previous studies, we have demonstrated that BBB leakage is reduced at 28 days after ablating a small subset of astrocytes *in vivo*. Even though tight junction function was disrupted at that timepoint, we observe the formation of glial boundaries adjacent to the sites of astrocyte ablation via increased astrocytic process length and volume, making glial boundary formation one possible mechanism for BBB repair after astrocyte ablation (Heithoff et al., 2021). When comparing how astrocytes respond to mTBI, we do not see glial boundary formation near areas containing atypical astrocytes. Thus, our mTBI data suggest that atypical astrocytes in mTBI may yield worse consequences than astrocyte ablation due to the combination of lack of glial boundary formation and reduced astrocyte-secreted factors, contributing to prolonged BBB leakage.

Overall, I established that mTBI triggers an atypical astrocyte response via leakage of blood-borne factors after BBB damage. Additionally, I developed a serum-free astrocyte cell culture model and identified two possible blood-borne factors that initiate this phenotype *in vitro*. Thus, developing therapeutic targets against the downstream signaling pathways in astrocytes that correspond to specific blood-borne factors that enter the brain parenchyma may serve to halt the progression of the neurological consequences observed after mTBI.

5 References

Akazawa-Ogawa, Y., Nagai, H., & Hagihara, Y. (2018). Heat denaturation of the antibody, a multi-domain protein. *Biophys Rev, 10*(2), 255-258. doi:10.1007/s12551-017-0361-8

Allahyari, R. V., Clark, K. L., Shepard, K. A., & Garcia, A. D. R. (2019). Sonic hedgehog signaling is negatively regulated in reactive astrocytes after forebrain stab injury. *Sci Rep, 9*(1), 565. doi:10.1038/s41598-018-37555-x

Allen, N. J., & Eroglu, C. (2017). Cell Biology of Astrocyte-Synapse Interactions. *Neuron, 96*(3), 697-708. doi:10.1016/j.neuron.2017.09.056

Alvarez, J. I., Dodelet-Devillers, A., Kebir, H., Ifergan, I., Fabre, P. J., Terouz, S., . . . Prat, A. (2011). The Hedgehog pathway promotes blood-brain barrier integrity and CNS immune quiescence. *Science, 334*(6063), 1727-1731. doi:10.1126/science.1206936

Annese, T., Corsi, P., Ruggieri, S., Tamma, R., Marinaccio, C., Picocci, S., . . . Nico, B. (2016). Isolation and characterization of neural stem cells from dystrophic mdx mouse. *Exp Cell Res, 343*(2), 190-207. doi:10.1016/j.yexcr.2016.03.019

Bolton-Hall, A. N., Hubbard, W. B., & Saatman, K. E. (2019). Experimental Designs for Repeated Mild Traumatic Brain Injury: Challenges and Considerations. *J Neurotrauma, 36*(8), 1203-1221. doi:10.1089/neu.2018.6096

Brimberg, L., Mader, S., Fujieda, Y., Arinuma, Y., Kowal, C., Volpe, B. T., & Diamond, B. (2015). Antibodies as Mediators of Brain Pathology. *Trends Immunol, 36*(11), 709-724. doi:10.1016/j.it.2015.09.008

Brown, J. M., Bentsen, M. A., Rausch, D. M., Phan, B. A., Wieck, D., Wasanwala, H., . . . Scarlett, J. M. (2021). Role of hypothalamic MAPK/ERK signaling and central action of FGF1 in diabetes remission. *iScience, 24*(9), 102944. doi:10.1016/j.isci.2021.102944

Bush, T. G., Puvanachandra, N., Horner, C. H., Polito, A., Ostenfeld, T., Svendsen, C. N., . . . Sofroniew, M. V. (1999). Leukocyte infiltration, neuronal degeneration, and neurite outgrowth after ablation of scar-forming, reactive astrocytes in adult transgenic mice. *Neuron, 23*(2), 297-308. doi:10.1016/s0896-6273(00)80781-3

Bylicky, M. A., Mueller, G. P., & Day, R. M. (2018). Mechanisms of Endogenous Neuroprotective Effects of Astrocytes in Brain Injury. *Oxid Med Cell Longev, 2018*, 6501031. doi:10.1155/2018/6501031

Cash, A., & Theus, M. H. (2020). Mechanisms of Blood-Brain Barrier Dysfunction in Traumatic Brain Injury. *Int J Mol Sci, 21*(9). doi:10.3390/ijms21093344

Cassidy, J. D., Carroll, L. J., Peloso, P. M., Borg, J., von Holst, H., Holm, L., . . . Coronado, V. G. (2004). Incidence, risk factors and prevention of mild traumatic brain injury: results of the WHO Collaborating Centre Task Force on Mild Traumatic Brain Injury. *J Rehabil Med*(43 Suppl), 28-60. doi:10.1080/16501960410023732

Chen, L., Wang, J., You, Q., He, S., Meng, Q., Gao, J., . . . Xu, Q. (2018). Activating AMPK to Restore Tight Junction Assembly in Intestinal Epithelium and to Attenuate Experimental Colitis by Metformin. *Front Pharmacol, 9*, 761. doi:10.3389/fphar.2018.00761

Clark, A. T., Abrahamson, E. E., Harper, M. M., & Ikonomovic, M. D. (2022). Chronic effects of blast injury on the microvasculature in a transgenic mouse model of Alzheimer's disease related Aβ amyloidosis. *Fluids Barriers CNS, 19*(1), 5. doi:10.1186/s12987-021-00301-z

Clark, V. D., Layson, A., Charkviani, M., Muradashvili, N., & Lominadze, D. (2018). Hyperfibrinogenemia-mediated astrocyte activation. *Brain Res, 1699*, 158-165. doi:10.1016/j.brainres.2018.08.023

D'Mello, S. R., & Kindy, M. C. (2020). Overdosing on iron: Elevated iron and degenerative brain disorders. *Exp Biol Med (Maywood), 245*(16), 1444-1473. doi:10.1177/1535370220953065

Davalos, D., Ryu, J. K., Merlini, M., Baeten, K. M., Le Moan, N., Petersen, M. A., . . . Akassoglou, K. (2012). Fibrinogen-induced perivascular microglial clustering is required for the development of axonal damage in neuroinflammation. *Nat Commun, 3*, 1227. doi:10.1038/ncomms2230

David, Y., Cacheaux, L. P., Ivens, S., Lapilover, E., Heinemann, U., Kaufer, D., & Friedman, A. (2009). Astrocytic dysfunction in epileptogenesis: consequence of altered potassium and glutamate homeostasis? *J Neurosci, 29*(34), 10588-10599. doi:10.1523/jneurosci.2323-09.2009

Derynck, R., & Budi, E. H. (2019). Specificity, versatility, and control of TGF-β family signaling. *Sci Signal, 12*(570). doi:10.1126/scisignal.aav5183

Ellis, M. J., Leddy, J., Cordingley, D., & Willer, B. (2018). A Physiological Approach to Assessment and Rehabilitation of Acute Concussion in Collegiate and Professional Athletes. *Front Neurol, 9*, 1115. doi:10.3389/fneur.2018.01115

Fehily, B., & Fitzgerald, M. (2017). Repeated Mild Traumatic Brain Injury: Potential Mechanisms of Damage. *Cell Transplant, 26*(7), 1131-1155. doi:10.1177/0963689717714092

Frigerio, F., Frasca, A., Weissberg, I., Parrella, S., Friedman, A., Vezzani, A., & Noé, F. M. (2012). Long-lasting pro-ictogenic effects induced in vivo by rat brain exposure to serum albumin in the absence of concomitant pathology. *Epilepsia, 53*(11), 1887-1897. doi:10.1111/j.1528-1167.2012.03666.x

Frik, J., Merl-Pham, J., Plesnila, N., Mattugini, N., Kjell, J., Kraska, J., . . . Götz, M. (2018). Cross-talk between monocyte invasion and astrocyte proliferation regulates scarring in brain injury. *EMBO Rep, 19*(5). doi:10.15252/embr.201745294

Gama Sosa, M. A., De Gasperi, R., Perez Garcia, G. S., Perez, G. M., Searcy, C., Vargas, D., . . . Elder, G. A. (2019). Low-level blast exposure disrupts gliovascular and neurovascular connections and induces a chronic vascular pathology in rat brain. *Acta Neuropathol Commun, 7*(1), 6. doi:10.1186/s40478-018-0647-5

Heinemann, U., Kaufer, D., & Friedman, A. (2012). Blood-brain barrier dysfunction, TGFβ signaling, and astrocyte dysfunction in epilepsy. *Glia, 60*(8), 1251-1257. doi:10.1002/glia.22311

Heithoff, B. P., George, K. K., Phares, A. N., Zuidhoek, I. A., Munoz-Ballester, C., & Robel, S. (2021). Astrocytes are necessary for blood-brain barrier maintenance in the adult mouse brain. *Glia, 69*(2), 436-472. doi:10.1002/glia.23908

Hoddevik, E. H., Rao, S. B., Zahl, S., Boldt, H. B., Ottersen, O. P., & Amiry-Moghaddam, M. (2020). Organisation of extracellular matrix proteins laminin and agrin in pericapillary basal laminae in mouse brain. *Brain Struct Funct, 225*(2), 805-816. doi:10.1007/s00429-020-02036-3

Holt, L. M., & Olsen, M. L. (2016). Novel Applications of Magnetic Cell Sorting to Analyze Cell-Type Specific Gene and Protein Expression in the Central Nervous System. *PLoS One, 11*(2), e0150290. doi:10.1371/journal.pone.0150290

Holt, L. M., Stoyanof, S. T., & Olsen, M. L. (2019). Magnetic Cell Sorting for In Vivo and In Vitro Astrocyte, Neuron, and Microglia Analysis. *Curr Protoc Neurosci, 88*(1), e71. doi:10.1002/cpns.71

Ivanova, A., Signore, M., Caro, N., Greene, N. D., Copp, A. J., & Martinez-Barbera, J. P. (2005). In vivo genetic ablation by Cre-mediated expression of diphtheria toxin fragment A. *Genesis, 43*(3), 129-135. doi:10.1002/gene.20162

Janigro, D. (2012). Are you in or out? Leukocyte, ion, and neurotransmitter permeability across the epileptic blood-brain barrier. *Epilepsia, 53 Suppl 1*(0 1), 26-34. doi:10.1111/j.1528-1167.2012.03472.x

Johnson, V. E., Stewart, J. E., Begbie, F. D., Trojanowski, J. Q., Smith, D. H., & Stewart, W. (2013). Inflammation and white matter degeneration persist for years after a single traumatic brain injury. *Brain, 136*(Pt 1), 28-42. doi:10.1093/brain/aws322

Kenzie, E. S., Parks, E. L., Bigler, E. D., Wright, D. W., Lim, M. M., Chesnutt, J. C., . . . Wakeland, W. (2018). The Dynamics of Concussion: Mapping Pathophysiology, Persistence, and Recovery With Causal-Loop Diagramming. *Front Neurol, 9*, 203. doi:10.3389/fneur.2018.00203

Kubotera, H., Ikeshima-Kataoka, H., Hatashita, Y., Allegra Mascaro, A. L., Pavone, F. S., & Inoue, T. (2019). Astrocytic endfeet re-cover blood vessels after removal by laser ablation. *Sci Rep, 9*(1), 1263. doi:10.1038/s41598-018-37419-4

Lee, S. W., Kim, W. J., Choi, Y. K., Song, H. S., Son, M. J., Gelman, I. H., . . . Kim, K. W. (2003). SSeCKS regulates angiogenesis and tight junction formation in blood-brain barrier. *Nat Med, 9*(7), 900-906. doi:10.1038/nm889

Leitner, L., El-Shabrawi, J. H., Bratschitsch, G., Eibinger, N., Klim, S., Leithner, A., & Puchwein, P. (2021). Risk adapted diagnostics and hospitalization following mild traumatic brain injury. *Arch Orthop Trauma Surg, 141*(4), 619-627. doi:10.1007/s00402-020-03545-w

Li, W., Long, J. A., Watts, L. T., Jiang, Z., Shen, Q., Li, Y., & Duong, T. Q. (2014). A quantitative MRI method for imaging blood-brain barrier leakage in experimental traumatic brain injury. *PLoS One, 9*(12), e114173. doi:10.1371/journal.pone.0114173

Lin, C. C., Lee, I. T., Wu, W. B., Liu, C. J., Hsieh, H. L., Hsiao, L. D., . . . Yang, C. M. (2013). Thrombin mediates migration of rat brain astrocytes via PLC, Ca^{2+}, CaMKII, PKCα, and AP-1-dependent matrix metalloproteinase-9 expression. *Mol Neurobiol, 48*(3), 616-630. doi:10.1007/s12035-013-8450-6

Marmarou, A., Foda, M. A., van den Brink, W., Campbell, J., Kita, H., & Demetriadou, K. (1994). A new model of diffuse brain injury in rats. Part I: Pathophysiology and biomechanics. *J Neurosurg, 80*(2), 291-300. doi:10.3171/jns.1994.80.2.0291

Mhatre, M., Nguyen, A., Kashani, S., Pham, T., Adesina, A., & Grammas, P. (2004). Thrombin, a mediator of neurotoxicity and memory impairment. *Neurobiol Aging, 25*(6), 783-793. doi:10.1016/j.neurobiolaging.2003.07.007

Michinaga, S., & Koyama, Y. (2019). Dual Roles of Astrocyte-Derived Factors in Regulation of Blood-Brain Barrier Function after Brain Damage. *Int J Mol Sci, 20*(3). doi:10.3390/ijms20030571

Moman, R. N., Gupta, N., & Varacallo, M. (2021). Physiology, Albumin. In *StatPearls*. Treasure Island (FL): StatPearls Publishing

Muñoz-Ballester, C., Mahmutovic, D., Rafiqzad, Y., Korot, A., & Robel, S. (2022). Mild Traumatic Brain Injury-Induced Disruption of the Blood-Brain Barrier Triggers an Atypical Neuronal Response. *Front. Cell. Neurosci.* doi.org/10.3389/fncel.2022.821885

Nakamura, M., Kaneko, S., Wate, R., Asayama, S., Nakamura, Y., Fujita, K., . . . Kusaka, H. (2013). Regionally different immunoreactivity for Smurf2 and pSmad2/3 in TDP-43-positive inclusions of amyotrophic lateral sclerosis. *Neuropathol Appl Neurobiol, 39*(2), 144-156. doi:10.1111/j.1365-2990.2012.01270.x

Nation, D. A., Sweeney, M. D., Montagne, A., Sagare, A. P., D'Orazio, L. M., Pachicano, M., . . . Zlokovic, B. V. (2019). Blood-brain barrier breakdown is an early biomarker of human cognitive dysfunction. *Nat Med, 25*(2), 270-276. doi:10.1038/s41591-018-0297-y

Nettis, M. A., & Pariante, C. M. (2020). Is there neuroinflammation in depression? Understanding the link between the brain and the peripheral immune system in depression. *Int Rev Neurobiol, 152*, 23-40. doi:10.1016/bs.irn.2019.12.004

Nguyen, T. S., Winn, H. R., & Janigro, D. (2000). ATP-sensitive potassium channels may participate in the coupling of neuronal activity and cerebrovascular tone. *Am J Physiol Heart Circ Physiol, 278*(3), H878-885. doi:10.1152/ajpheart.2000.278.3.H878

Obermeier, B., Daneman, R., & Ransohoff, R. M. (2013). Development, maintenance and disruption of the blood-brain barrier. *Nat Med, 19*(12), 1584-1596. doi:10.1038/nm.3407

Pannasch, U., & Rouach, N. (2013). Emerging role for astroglial networks in information processing: from synapse to behavior. *Trends Neurosci, 36*(7), 405-417. doi:10.1016/j.tins.2013.04.004

Parasuraman, S., Raveendran, R., & Kesavan, R. (2010). Blood sample collection in small laboratory animals. *J Pharmacol Pharmacother, 1*(2), 87-93. doi:10.4103/0976-500x.72350

Pardridge, W. M., Boado, R. J., & Farrell, C. R. (1990). Brain-type glucose transporter (GLUT-1) is selectively localized to the blood-brain barrier. Studies with quantitative western blotting and in situ hybridization. *J Biol Chem, 265*(29), 18035-18040.

Pavlovic, D., Pekic, S., Stojanovic, M., & Popovic, V. (2019). Traumatic brain injury: neuropathological, neurocognitive and neurobehavioral sequelae. *Pituitary, 22*(3), 270-282. doi:10.1007/s11102-019-00957-9

Pedrazzani, C., Mantovani, G., Salvagno, G. L., Baldiotti, E., Ruzzenente, A., Iacono, C., . . . Guglielmi, A. (2016). Elevated fibrinogen plasma level is not an independent predictor of poor prognosis in a large cohort of Western patients undergoing surgery for colorectal cancer. *World J Gastroenterol, 22*(45), 9994-10001. doi:10.3748/wjg.v22.i45.9994

Petersen, M. A., Ryu, J. K., & Akassoglou, K. (2018). Fibrinogen in neurological diseases: mechanisms, imaging and therapeutics. *Nat Rev Neurosci, 19*(5), 283-301. doi:10.1038/nrn.2018.13

Piao, C. S., Holloway, A. L., Hong-Routson, S., & Wainwright, M. S. (2019). Depression following traumatic brain injury in mice is associated with down-regulation of hippocampal astrocyte glutamate transporters by thrombin. *J Cereb Blood Flow Metab, 39*(1), 58-73. doi:10.1177/0271678x17742792

Ralay Ranaivo, H., Hodge, J. N., Choi, N., & Wainwright, M. S. (2012). Albumin induces upregulation of matrix metalloproteinase-9 in astrocytes via MAPK and reactive oxygen species-dependent pathways. *J Neuroinflammation, 9*, 68. doi:10.1186/1742-2094-9-68

Ralay Ranaivo, H., & Wainwright, M. S. (2010). Albumin activates astrocytes and microglia through mitogen-activated protein kinase pathways. *Brain Res, 1313*, 222-231. doi:10.1016/j.brainres.2009.11.063

Ransohoff, R. M., Schafer, D., Vincent, A., Blachère, N. E., & Bar-Or, A. (2015). Neuroinflammation: Ways in Which the Immune System Affects the Brain. *Neurotherapeutics, 12*(4), 896-909. doi:10.1007/s13311-015-0385-3

Reis, G. B., Rees, J. C., Ivanova, A. A., Kuklenyik, Z., Drew, N. M., Pirkle, J. L., & Barr, J. R. (2021). Stability of lipids in plasma and serum: Effects of temperature-related storage conditions on the human lipidome. *J Mass Spectrom Adv Clin Lab, 22*, 34-42. doi:10.1016/j.jmsacl.2021.10.002

Robel, S., Buckingham, S. C., Boni, J. L., Campbell, S. L., Danbolt, N. C., Riedemann, T., . . . Sontheimer, H. (2015). Reactive astrogliosis causes the development of spontaneous seizures. *J Neurosci, 35*(8), 3330-3345. doi:10.1523/jneurosci.1574-14.2015

Schachtrup, C., Ryu, J. K., Helmrick, M. J., Vagena, E., Galanakis, D. K., Degen, J. L., . . . Akassoglou, K. (2010). Fibrinogen triggers astrocyte scar formation by promoting the availability of active TGF-beta after vascular damage. *J Neurosci, 30*(17), 5843-5854. doi:10.1523/jneurosci.0137-10.2010

Senatorov, V. V., Jr., Friedman, A. R., Milikovsky, D. Z., Ofer, J., Saar-Ashkenazy, R., Charbash, A., . . . Kaufer, D. (2019). Blood-brain barrier dysfunction in aging induces hyperactivation of TGFβ signaling and chronic yet reversible neural dysfunction. *Sci Transl Med, 11*(521). doi:10.1126/scitranslmed.aaw8283

Shandra, O., & Robel, S. (2019). Imaging and Manipulating Astrocyte Function In Vivo in the Context of CNS Injury. *Methods Mol Biol, 1938*, 233-246. doi:10.1007/978-1-4939-9068-9_16

Shandra, O., Winemiller, A. R., Heithoff, B. P., Munoz-Ballester, C., George, K. K., Benko, M. J., . . . Robel, S. (2019). Repetitive Diffuse Mild Traumatic Brain Injury Causes an Atypical Astrocyte Response and Spontaneous Recurrent Seizures. *J Neurosci, 39*(10), 1944-1963. doi:10.1523/jneurosci.1067-18.2018

Sharma, S., Tiarks, G., Haight, J., & Bassuk, A. G. (2021). Neuropathophysiological Mechanisms and Treatment Strategies for Post-traumatic Epilepsy. *Front Mol Neurosci, 14*, 612073. doi:10.3389/fnmol.2021.612073

Sivandzade, F., Alqahtani, F., & Cucullo, L. (2020). Traumatic Brain Injury and Blood-Brain Barrier (BBB): Underlying Pathophysiological Mechanisms and the Influence of Cigarette Smoking as a Premorbid Condition. *Int J Mol Sci, 21*(8). doi:10.3390/ijms21082721

Sofroniew, M. V. (2009). Molecular dissection of reactive astrogliosis and glial scar formation. *Trends Neurosci, 32*(12), 638-647. doi:10.1016/j.tins.2009.08.002

Some, D., Amartely, H., Tsadok, A., & Lebendiker, M. (2019). Characterization of Proteins by Size-Exclusion Chromatography Coupled to Multi-Angle Light Scattering (SEC-MALS). *J Vis Exp*(148). doi:10.3791/59615

Sulimai, N., & Lominadze, D. (2020). Fibrinogen and Neuroinflammation During Traumatic Brain Injury. *Mol Neurobiol, 57*(11), 4692-4703. doi:10.1007/s12035-020-02012-2

Szarka, N., Toth, L., Czigler, A., Kellermayer, Z., Ungvari, Z., Amrein, K., . . . Toth, P. (2019). Single Mild Traumatic Brain Injury Induces Persistent Disruption of the Blood-Brain Barrier, Neuroinflammation and Cognitive Decline in Hypertensive Rats. *Int J Mol Sci, 20*(13). doi:10.3390/ijms20133223

Tagge, C. A., Fisher, A. M., Minaeva, O. V., Gaudreau-Balderrama, A., Moncaster, J. A., Zhang, X. L., . . . Goldstein, L. E. (2018). Concussion, microvascular injury, and early tauopathy in young athletes

after impact head injury and an impact concussion mouse model. *Brain, 141*(2), 422-458. doi:10.1093/brain/awx350

Tamma, R., Annese, T., Capogrosso, R. F., Cozzoli, A., Benagiano, V., Sblendorio, V., . . . Nico, B. (2013). Effects of prednisolone on the dystrophin-associated proteins in the blood-brain barrier and skeletal muscle of dystrophic mdx mice. *Lab Invest, 93*(5), 592-610. doi:10.1038/labinvest.2013.46

Tecalco-Cruz, A. C., Ríos-López, D. G., Vázquez-Victorio, G., Rosales-Alvarez, R. E., & Macías-Silva, M. (2018). Transcriptional cofactors Ski and SnoN are major regulators of the TGF-β/Smad signaling pathway in health and disease. *Signal Transduct Target Ther, 3*, 15. doi:10.1038/s41392-018-0015-8

van de Haar, H. J., Burgmans, S., Jansen, J. F., van Osch, M. J., van Buchem, M. A., Muller, M., . . . Backes, W. H. (2016). Blood-Brain Barrier Leakage in Patients with Early Alzheimer Disease. *Radiology, 281*(2), 527-535. doi:10.1148/radiol.2016152244

Vazquez, R., & Larson, D. F. (2013). Plasma protein denaturation with graded heat exposure. *Perfusion, 28*(6), 557-559. doi:10.1177/0267659113498921

Wan, J., Ren, H., & Wang, J. (2019). Iron toxicity, lipid peroxidation and ferroptosis after intracerebral haemorrhage. *Stroke Vasc Neurol, 4*(2), 93-95. doi:10.1136/svn-2018-000205

Wiethoff, S., & Houlden, H. (2017). Neurodegeneration with brain iron accumulation. *Handb Clin Neurol, 145*, 157-166. doi:10.1016/b978-0-12-802395-2.00011-0

Xing, G., Zhao, T., Zhang, X., Li, H., Li, X., Cui, P., . . . Jiang, W. (2020). Astrocytic Sonic Hedgehog Alleviates Intracerebral Hemorrhagic Brain Injury via Modulation of Blood-Brain Barrier Integrity. *Front Cell Neurosci, 14*, 575690. doi:10.3389/fncel.2020.575690

Xu, L., Nirwane, A., & Yao, Y. (2019). Basement membrane and blood-brain barrier. *Stroke Vasc Neurol, 4*(2), 78-82. doi:10.1136/svn-2018-000198

Xu, Y., He, Q., Wang, M., Wang, X., Gong, F., Bai, L., . . . Wang, W. (2019). Quantifying blood-brain-barrier leakage using a combination of evans blue and high molecular weight FITC-Dextran. *J Neurosci Methods, 325*, 108349. doi:10.1016/j.jneumeth.2019.108349

Yao, L., Xue, X., Yu, P., Ni, Y., & Chen, F. (2018). Evans Blue Dye: A Revisit of Its Applications in Biomedicine. *Contrast Media Mol Imaging, 2018*, 7628037. doi:10.1155/2018/7628037

Yu, X., Ji, C., & Shao, A. (2020). Neurovascular Unit Dysfunction and Neurodegenerative Disorders. *Front Neurosci, 14*, 334. doi:10.3389/fnins.2020.00334

Zhang, R., Wu, Y., Xie, F., Zhong, Y., Wang, Y., Xu, M., . . . Qin, X. (2018). RGMa mediates reactive astrogliosis and glial scar formation through TGFβ1/Smad2/3 signaling after stroke. *Cell Death Differ, 25*(8), 1503-1516. doi:10.1038/s41418-018-0058-y

Zhu, S. L., Luo, M. Q., Peng, W. X., Li, Q. X., Feng, Z. Y., Li, Z. X., . . . Huang, J. L. (2015). Sonic hedgehog signalling pathway regulates apoptosis through Smo protein in human umbilical vein endothelial cells. *Rheumatology (Oxford), 54*(6), 1093-1102. doi:10.1093/rheumatology/keu421